ELASTIC-PLASTIC FINITE ELEMENT MODELING OF LONG SPAN COMPOSITE JOISTS WITH INCOMPLETE INTERACTION

by

Son T. Nguyen

Thesis submitted to the faculty of the
Virginia Polytechnic Institute and State University
in partial fulfillment of the requirements for the degree of
MASTER OF SCIENCE
in
Civil Engineering

APPROVED:

W. Samuel Easterling, Chairman

Thomas M. Murray

Siegfried M. Holzer

May 1992

Blacksburg, VA 24061

ELASTIC-PLASTIC FINITE ELEMENT MODELING OF LONG SPAN COMPOSITE JOISTS WITH INCOMPLETE INTERACTION

by
Son T. Nguyen

Committee Chairman: Dr. W. Samuel Easterling
Civil Engineering

(ABSTRACT)

This thesis presents elastic-plastic finite element analyses of seven long span composite open-web steel joists. These analyses account for the incomplete interaction between the concrete slab and the steel joist by modeling the nonlinear behavior of the steel shear connectors.

Experimental tests on long span composite open-web steel joists were performed at Virginia Polytechnic Institute and State University. Measurements of joist deflections, member strains, and slip between the concrete slab and steel joist were recorded.

The response of the finite element models agree reasonably well with the response of the test prototypes where the shear connector position was known. The finite element model can be generated on any general purpose finite element program that includes beam elements and nonlinear spring elements. The finite element model can give reasonable predictions of deflections and ultimate load capacity of a composite open-web steel joist.

ACKNOWLEDGMENTS

I would like to thank Dr. W. Samuel Easterling for his patience and guidance through the experimental and analytical portions of this study. I would also like to thank Dr. Thomas M. Murray for the opportunity to work with him on this and other projects and for serving on my committee. Thanks are also owed to Dr. Siegfried Holzer for his ideas and suggestion on the finite element modeling and, more importantly, for his holistic advice on graduate life.

Many thanks are also owed to my fellow graduate students who assisted me in the construction and testing of the composite joists, David McGowan, Doug Lauer, Bruce Queen, Archie Pugh, Steve Hanagan, and David Gibbings. I would also like to thank Dennis Huffman and Brett Farmer for providing their skill and workmanship in helping construct and test the composite joists.

A special thanks goes to NUCOR Research and Development, a division of NUCOR, for funding the experimental part of this study.

Finally, I thank my parents for inspiring me to learn at an early age and to those teachers I've had in the past who have made it possible for me to go this far in my education.

TABLE OF CONTENTS

LIST OF FIGURES

LIST OF TABLES

CHAPTER I

INTRODUCTION

1.1 Background

Steel and concrete structures have been used compositely in many structural designs to take advantage of the higher strength and stiffness of the two materials acting together versus each material acting alone. Composite members typically possess significant ductility, a characteristic which makes them good choices for seismic design applications.

Composite action is achieved by using a form of shear connection at the steel-concrete interface. Shear connectors can be of various shapes and sizes. The most common form of shear connector used in the United States for joist and beam applications is the headed shear stud. This type of shear connection is the only type of shear connector considered in this report.

The composite joist has many advantages over the composite beam including the ability to span longer lengths, usually at lower material costs. Another advantage of composite joists is that electrical and mechanical services can be routed through the web of the joist whereas they would have to be placed under a composite beam or web openings would have to be cut in the beam, adding cost to the structure.

Despite the advantages of composite open-web steel joists, their use in building structures has only become popular in the last five years. Composite beams are more widely used in design because more analysis

and design procedures have been developed for these members. No nationally accepted standard exists in the U.S. for the design of composite joists. The only published book which gives guidelines for the design of composite joists is by Chien and Ritchie (1984) which complies with the Canadian Institute of Steel Construction's Limit States Design Code (1984). The development of a finite element model for composite open-web steel joists will add to the tools available for the analysis and design of these members.

1.2 Experimental Studies

Eleven long span composite open-web steel joists were tested to failure at Virginia Tech (Gibbings, et al. 1991; Nguyen, et al. 1991). Seven of the eleven tests were used in this finite element study. The seven tests were chosen because the shear stud positions relative to the deck profile of these tests were known. The shear stud position plays an important role in the modeling process as this report will describe.

Measurements of joist deflections, member strains, and slip between the concrete slab and the steel joist were recorded and reduced for the experimental tests. The experimental deflection, strain, and slip measurements will be compared to the finite element results.

1.3 Scope of Research

The objective of this research was to develop an accurate finite element model for long span composite joists. Seven experimental models

were used to validate and modify the modeling techniques taking into account the flexibility in the shear connectors and elastic-plastic material behavior. A general purpose finite element package (ANSYS) was used as the analysis tool.

The results of the finite element analyses were obtained. The accuracy of the finite element models in predicting the composite joist deflection and ultimate load was evaluated. Recommendations for the finite element modeling approach and possible future studies were made.

CHAPTER II

LITERATURE REVIEW

2.1 Introduction

Finite element analysis has been used to study the behavior of structures for about the last thirty-five years. The finite element method was first proposed by Courant (1943). The first use of the finite element method in this country was by Turner et al. (1956) for aerospace applications. Almost at the same time, Argyris (1960) published independent research on the application of the finite element method to aircraft structures. Since then, the finite element method has been applied to many other disciplines. One of the disciplines that makes widespread use of the finite element method is the analysis of building structures. Only literature pertaining to steel-concrete composite structures will be reviewed.

2.2 Finite Element Analysis of Steel-Concrete Composite Structures

Hamada and Arizumi (1977) performed elastic analyses of continuous composite beams. Their finite element model accounted for incomplete interaction between the concrete slab and the steel beam by using experimental data from push out tests for the shear force-slip behavior of the shear connectors. Incomplete interaction refers to the flexibility in the shear connectors due to deformation under load. The results obtained by Hamada and Arizumi showed good agreement between the model and the

exact values of deflection calculated by Newmark, et al. (1951). The exact solutions by Newmark, et al. account for incomplete interaction in the composite joist by a differential equation developed by Newmark.

Hirst and Yeo (1980) performed elastic and ultimate load analyses of composite beams using a standard finite element program available at the University of Adelaide. Their model accounted for the shear and bending in the shear connectors. The incomplete interaction model used in the study incorporates a stiffness relation for the shear connectors derived from simple beam theory. Each shear connector was modeled as two connecting elements at the two nodes nearest the actual shear connector location. The finite element model presented by Hirst and Yeo permits modeling of partial interaction. However, the ultimate load values obtained, based on partial interaction, underpredicted the experimental values.

Arizumi and Hamada (1981) performed elastic-plastic finite element analyses of composite beams with incomplete interaction. In their previous study (Hamada and Arizumi 1977), the connectors were assumed to behave linearly because only the elastic behavior of the composite beams were desired. In their 1981 study, the shear connectors were modeled with an idealized elastic-plastic stress-strain relationship. The other components of the composite beam were also modeled with the elastic-plastic stress-strain relationship. Good agreement was obtained between the proposed model and the test results.

Razaqur and Nofal (1989) presented a finite element for modeling shear connectors in composite structures. Their three-dimensional bar finite element consists of two nodes with three translational degrees of freedom

at each node. The bar element accounts for shear and axial stiffness while neglecting the flexural and torsional stiffness of the shear connector. Yam and Chapman's empirical shear force-slip equation was used to model the shear deformation of the stud (Yam and Chapman 1972). Yam and Chapman's equation is:

$$F = a(1-e^{-bx}) \qquad (1.1)$$

where F = shear force on stud

x = relative slip between stud top and bottom

a,b = constants obtained from experimental data

e = base of natural logarithm

The shear connectors were modeled by two equivalent connectors at the two nearest nodal points. The stiffness of the two equivalent connectors were found in the same way as the equivalent nodal forces. The shear connector element was used to model the behavior of a simply supported beam and a continuous beam. The results of the models agreed reasonably well with the experimental values. The model of the simply supported beam had greater stiffness than the experimental test, but the ultimate strength of the model agreed well with that of the test. The results of the finite element model for the continuous beam also showed good agreement with the experimental values.

Razaqur and Nofal (1990) later developed a finite element program NONLACS (NONlinear Analysis of Concrete and Steel) to analyze composite structures in three dimensions. Razaqur and Nofal dealt mainly with modeling the nonlinear behavior of composite bridges. The shear connector element they developed earlier (Razaqur and Nofal 1989) was used in this

study. The shear connector accounts for the shear and axial stiffness but ignores the flexural and torsional stiffness. The authors (Razaqur and Nofal 1989) state that at failure, the combined shear and axial stiffness is ignored since studies (Johnson and Buckby 1986) have shown that the uplift force in the shear studs at failure is relatively negligible . The findings of their study indicate that the elastic and inelastic behavior of composite bridges can be reasonably modeled using a finite element program such as NONLACS. NONLACS can model steel yielding and concrete crushing, but not buckling. Consequently, accurate results cannot be guaranteed if the mode of failure is buckling. NONLACS is also limited to modeling thin plane members as shear deformation is not accounted for in its elements.

Kitoh and Sonoda (1991) conducted eight experimental tests on composite concrete slabs and performed three-dimensional finite element analyses on the concrete slabs. A point matching technique was used to model the continuity between the concrete slab and the steel plate. The point matching technique employed the nonlinear shear force-deflection relation of Ollgaard, et al. (1971). The Ollgaard, et al. equation is given by:

$$Q = Q_u(1-e^{-18x})^{2/3} \qquad (1.2)$$

where Q = shear force on stud

Q_u = ultimate shear capacity

x = relative slip between stud top and bottom

e = base of natural logarithm

An alternative model which incorporated an infinitely rigid connection between the concrete slab and the steel plate was also examined. Kitoh and Sonoda found that the stud forces obtained from the Ollgaard, et al.

gave much better agreement with the measured stud forces than the infinitely rigid connection. Kitoh and Sonoda also found from experimental tests that most of the shear force was carried by the welded base of the shear stud and the shank of the stud carried almost none of the shear.

Wegmuller and Amer (1977) studied the nonlinear behavior of composite steel-concrete bridges using three-dimensional finite element analyses. The nonlinear finite element analysis was used to study the behavior of the composite bridges at any level of overload. Overload is defined by Wegmuller (1977) as, "any load above the load that produces first yielding in a steel beam being examined." The slip between the concrete slab and the steel beams was not modeled in their analysis. The nonlinearity in the analyses came from modeling the steel and concrete as elastic-plastic members with the steel having the same properties in tension as in compression and the concrete acting in compression only up to crushing strain. Wegmuller and Amer reported favorable comparisons between the finite element model results and the experimental results.

In a companion study by Wegmuller (1977), the overload behavior of composite steel-concrete bridges was examined using the same finite element model described previously. Wegmuller varied the tensile strength of the concrete and found little difference in the structure stiffness. Wegmuller also examined the effect of varying the load increments from 5% to 10% of the yield load in the nonlinear region. Again he found little difference in the structural response. Wegmuller points out that the finite element model compares favorably with experimental results in the elastic

and postcracking range. The assumption that the concrete slab behaves elastic, perfectly-plastic works fairly well up to about 20% overload.

McCarthy and Melhem (1988) developed a finite element program to analyze the elastic and plastic behavior of composite steel-concrete superstructures. Analyses of composite bridges were performed to test the program. Models were analyzed using strain-hardening in the steel, no strain-hardening in the steel, and noncomposite steel. The models show that for structures where the plastic hinge formation is extensive, strain-hardening increases the ultimate load of the structure by a maximum of 10%.

McCarthy and Melhem accounted for the partial connection behavior in the composite structure by using a least squares formulation of experimental data to determine the structure's composite properties. The composite formulas based on the least squares approach gave conservative ultimate capacities in the range of 10%-20% under the experimental ultimate capacities. This is because the deck has to carry a significant portion of the load since the composite strength is not assigned to the deck. The results of the finite element models were reported to agree reasonably well with the experimental results.

2.3 Finite Element Analysis of Composite Open-Web Joists

A limited number of finite element studies on composite open-web steel joists have been conducted. Two studies were performed using frame analysis programs (Azmi 1972; Curry 1988). The analyses performed by

Azmi assumed that the connection between the concrete slab and the steel joist was rigid, which is not an accurate representation of the behavior of the shear connectors. Azmi's models were elastic thus not modeling the nonlinear behavior of the shear connectors and the steel joist.

Curry tried various methods to account for the slip between the concrete slab and the steel joist. Curry found that the best model used the relation developed by Ollgaard, et al. (1971) to calculate the properties of the shear stud using elastic beam theory. The model, however, could only describe the behavior of the composite joist at one load level. If the response of the composite joist were desired at another load level, the shear stud properties would have to be recalculated from the Ollgaard, et al. equation and the elastic deflection equation and entered into the program again.

Gibbings, et al. (1991) conducted a finite element analysis of a composite joist in which the plasticity of the steel was modeled, but again the shear connection between the concrete slab and the steel joist was assumed to be rigid. The finite element model response was slightly stiffer than the response of the test specimen. However, the ultimate load capacities of the finite element model and the specimen were in good agreement.

2.4 Concluding Remarks on Literature Review

Finite element models of composite structures in this literature survey had success using a nonlinear shear force-deformation relation such as that

of Yam and Chapman (1972) or Ollgaard, et al. (1971) to represent the shear stud behavior. Finite element models of composite joists up to now have been limited to elastic analysis and complete interaction, i.e. no slip between the concrete slab and the steel joist. Gibbings (1991) conducted a finite element analysis using elastic-plastic elements for the bottom chord of the steel joist, but assumed rigid connection between the concrete slab and the steel joist. Curry (1988) accounted for the slip between the concrete slab and the steel joist, but the method that was presented proved to be cumbersome for a range of elastic loads.

CHAPTER III

EXPERIMENTAL TESTING

3.1 Experimental Setup

The composite joists examined in this study were tested at Virginia Tech and reported by Gibbings, et al. (1991) and Nguyen, et al. (1991). The test setup was used to demonstrate the behavior of a typical composite joist span from center to center of the concrete slab. The ends of the joist were simply supported on beams. The test matrix of the seven composite joist tests is given in Table 3.1.

Tests CLH-5 through CLH-9 and CLH-11 were selected for modeling because their shear stud positions were known and were loaded to failure. CLH-4 was also modeled because the shear studs were believed to be placed in mostly weak positions, and modeling CLH-4 could provide additional insight into the behavior of the composite joists. The loading scheme used either a single hydraulic ram or a double hydraulic ram system. For the single hydraulic ram system, seven spreader beams were placed under the ram to spread the load over eight concentrated roller load points as shown in Figure 3.1. For the double hydraulic ram system, three spreader beams were placed under each ram to give a total of eight concentrated roller load points as shown in Figure 3.2. The single and double ram loading systems give the same loading since both rams of the double ram system are hydraulically operated by the same pump line and the two rams are the same size. The load on the two rams in the double

ram system was the same at any load point. This was verified by load readings on each ram from load cells place above the rams.

Table 3.1 Test Matrix

Test	Span (ft)	Joist Depth (in)	# of Studs	Slab Depth (in)	Rib Height (in)	Slab Width (in)	Stud Position
CLH-4	40	16	44	6	3	81	Mostly Weak[1]
CLH-5	40	34	22	6	3	81	Strong[2]
CLH-6	40	14	36	5	2	81	Strong[2]
CLH-7	40	20	36	5	2	81	Strong[2]
CLH-8	40	20	36	5	2	81	Strong[2]
CLH-9	40	32	22	6	2	81	Strong / Weak[3]
CLH-11	40	16	40	5	2	81	Strong / Weak[3]

[1] The studs were believed to be placed in the weak position with the exception of a few in the strong position. The precise locations were not documented

[2] The studs were all placed in the strong position

[3] The studs were alternated between the strong and weak positions

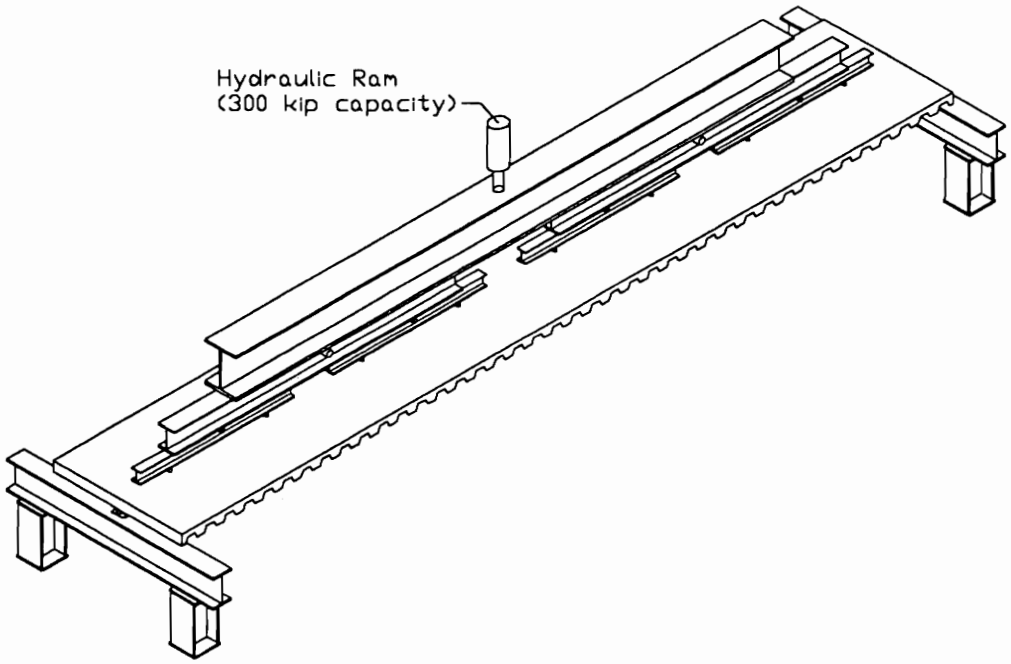

Figure 3.1 Single Ram Loading System

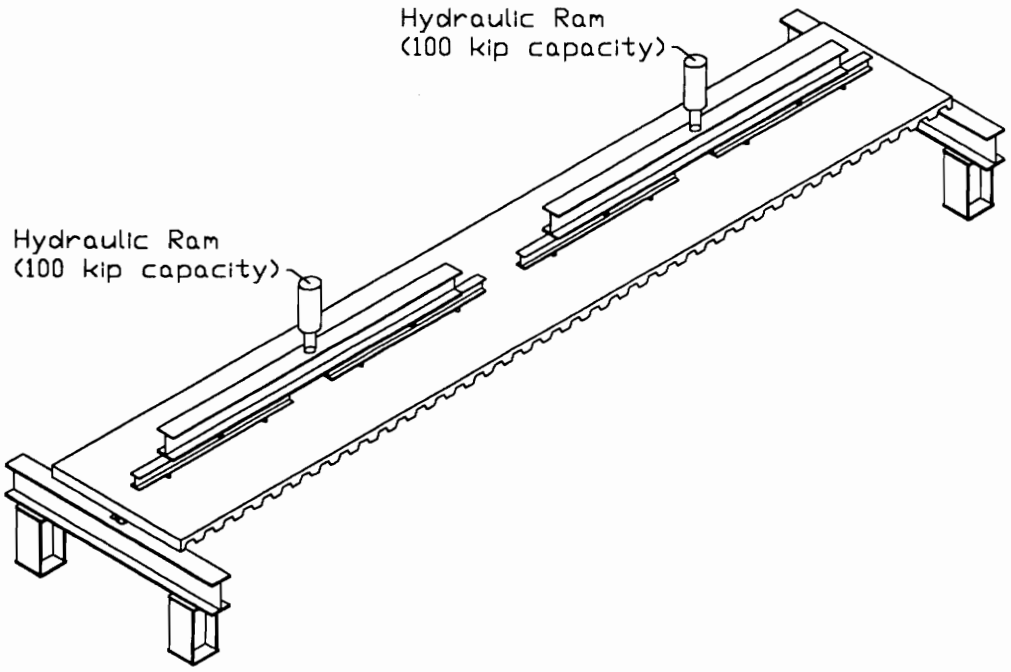

Figure 3.2 Double Ram Loading System

3.2 Composite Joist Nomenclature

The composite joist components are named and numbered as follows. The top chord refers to the top chord angles of the steel joist. The bottom chord refers to the bottom chord angles of the steel joist. The bottom chord angles are the main tension resisting component of the composite joist.

The web members are the diagonal or vertical members of the steel joist and are the members that resist the shear forces. The diagonal members are labeled with a W starting with 2 from one end and increasing in number to the midspan, e.g. W2. The opposite end of the joist follows the same numbering scheme, but an R is added at the end of the label, e.g. W2R.

The vertical web members may be either vertical or slightly skewed from the vertical. The verticals are labeled with a VR and a starting number of 2 and increasing from one end of the strain gaged side to the end of the non-strain gaged side. This labeling holds for all verticals except for the end verticals next to W2 and W2R. This end vertical is labeled 2DL on the strain gaged side and 2DLR on the non-strain gaged side. The vertical members were placed at panel points on the top chord where the point loads would be applied that did not coincide with a panel point. Figure 3.3 shows typical steel joist nomenclature used throughout this report.

Due to the presence of stiffening ribs in the bottom flange of the metal deck , the shear stud placement on the ribbed metal deck will have one of two positions. The weak stud position in the metal deck is on the side of the deck flute that is closest to the joist centerline as shown in

Figure 3.4. The strong stud position in the metal deck is on the side of the deck flute that is farthest away from the joist centerline.

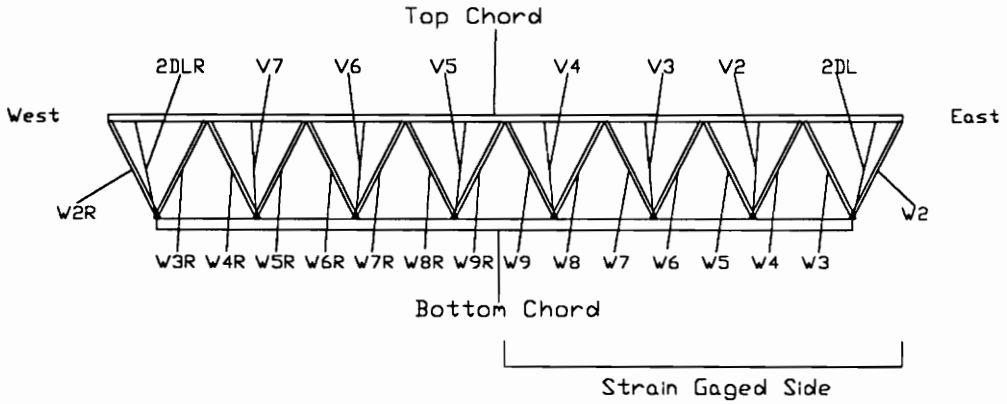

Figure 3.3 Typical Joist Nomenclature

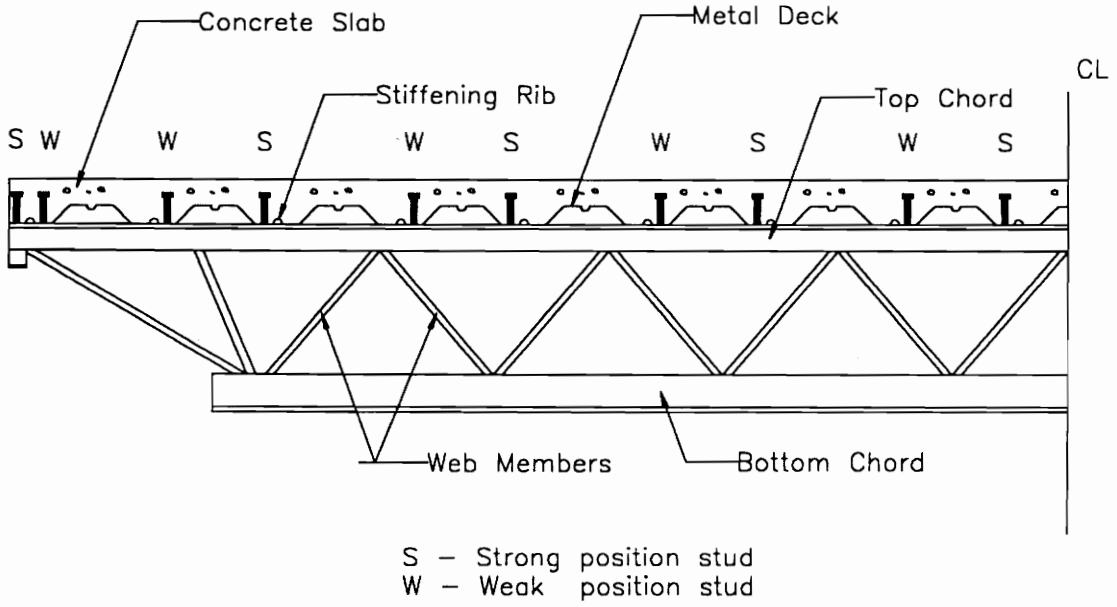

Figure 3.4 Shear Stud Positions

3.2 Experimental Instrumentation

Strain gages were placed on the top chord, the bottom chord, and various web members of the composite joist to record member strains during testing. Whenever possible, four strain gages were installed at a single cross section so that the member strains could be averaged to give an equivalent strain at the member neutral axis. For single angle web members, two strain gages were placed on the legs of the angle. It is sufficient to say that a minimum of two strain gages per location will give an accurate member strain if the strain gages are placed symmetrically about the member neutral axis so that the strain readings can be averaged. For the most part, four strain gages were used per location.

Vertical deflection transducers were placed at the steel joist quarterspan and centerline locations. Deflection transducers were attached to the top and bottom chords at each location. The deflection transducers measured the vertical displacement of the composite joist under load, as well as the distance between chords.

For every test, slip transducers or dial gages were installed at the ends of the composite joist. A slip transducer was also installed at the centerline of the composite joist for each test. Additional slip transducers were placed along one side of the joist centerline to measure the relative slip along the top chord of the joist. Figure 3.5 shows the schematic of the instrumentation locations for CLH-11 which is typical for all the tests.

Load cells were used to measure the applied load by the rams. The load cell was placed between the stationary load block and the hydraulic

ram. More details of the test instrumentation can be found in reports by Gibbings, et al. (1991) and Nguyen, et al. (1991).

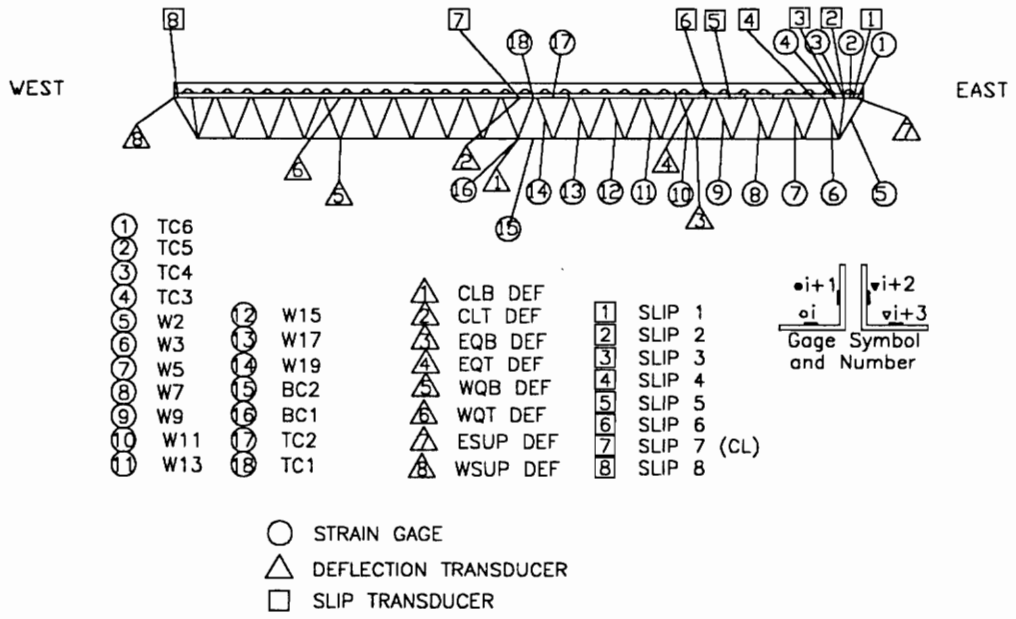

Figure 3.5 Schematic of Typical Instrumentation Locations

3.3 Experimental Results

Select experimental results from Gibbings, et al. (1991) and Nguyen, et al. (1991) are used in this report. Strain, deflection, and slip response curves for the composite section are used for comparison with the finite element results. The research reports may be consulted for complete experimental results.

CHAPTER IV

FINITE ELEMENT MODELING METHODS

4.1 Overview

Preliminary tests on analytical composite joist models must be performed to better understand the parameters involved in the modeling process. The variation of one or more parameters can have dramatic effects on the model response and may help to give more insight into the actual structural behavior. The best method of modeling the structure can be determined by comparing the response of the model to the response of the experimental specimen.

The shear stud is one of the more difficult components to model because of the interaction of steel and concrete at the interface. The shear stud behavior will determine the degree of composite action in the joist model. The degree of composite action will in turn determine the composite joist stiffness and ultimate load capacity. To see the effect of full composite action, the shear connectors can be modeled as infinitely stiff. Next, the shear connectors can be modeled using the actual stud properties based on the stud's diameter. Finally, the shear connectors can be modeled using an infinitely stiff beam element for the stud shank and a nonlinear spring element for the base of the stud. A shear force-deformation relationship can be used for the nonlinear spring to represent the shear stud stiffness.

The mesh of the finite element model was tested to see if it was sufficiently fine for modeling the prototype response. The convergence of the nonlinear spring element and the elastic-plastic beam element was examined. A plastic convergence criteria utilizing equilibrium was the final test of convergence for the model in the plastic region. A discussion of the convergence requirements will follow near the end of this chapter.

4.2 Modeling Assumptions

Certain assumptions are made in the finite element study to simplify the analysis. The beam elements are assumed doubly symmetric and prismatic in the finite element package ANSYS (Swanson 1989a). In the inelastic loading of the structure, the strain increment is assumed to be relatively small compared to the total strain in any member.

Simplifying assumptions were made in the modeling process. A two-dimensional model would be a good starting point for modeling the composite joist, since the internal and external forces on the structure are approximately planar. If a two-dimensional model is not sufficiently accurate for modeling the composite joist, a three-dimensional model may be required.

4.3 Modeling the Composite Joist Components

The steel joist web members and concrete slab were modeled as beam elements with the STIF3 element in ANSYS (Swanson 1989). The STIF3 element is a two-dimensional elastic beam element. The steel joist

top chord and bottom chord were modeled as plastic beam elements with the STIF23 element in ANSYS. The STIF23 element is a two-dimensional plastic beam element. The bilinear stress-strain curve of the plastic beam element is defined by specifying a yield stress and the modulus of elasticity of the element. The steel shear stud was modeled using the STIF3 beam element for the shaft of the stud and the STIF39 spring element was used to model the shear stiffness of the stud at its base. The STIF39 element is a nonlinear spring element. The nonlinear behavior of the spring element is defined by specifying up to 12 points on the load-displacement curve.

The modulus of elasticity used for the elements in the model was 29,000 ksi. The properties of the concrete slab were transformed into equivalent steel properties, so the modulus of elasticity of steel was used for the slab in the model. More details about the modeling of the composite joist components are given in the following sections. A typical finite element model is shown in Figure 4.1.

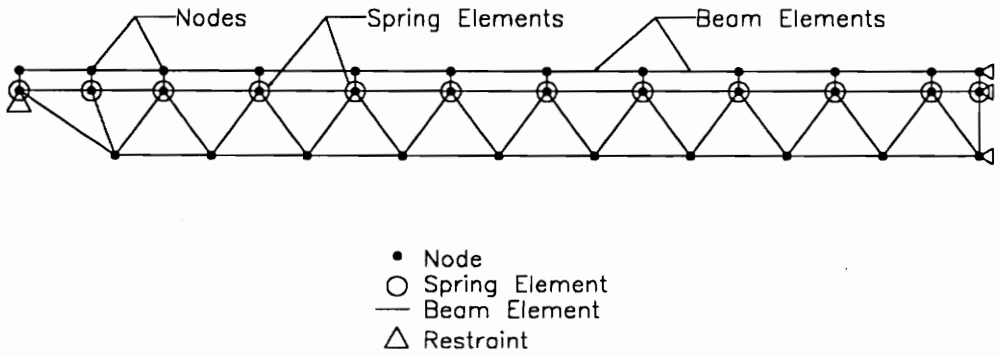

Figure 4.1 Typical Finite Element Model

4.3.1 Steel Joist Top and Bottom Chords

The yield stresses for the steel joist top and bottom chord members were calculated by accounting for the stresses due to concrete placement. This allows for direct comparison of the composite loading of the model and the prototype. The actual yield stresses were obtained from tensile coupon tests. In some cases, the top chord tensile coupon test data were not available so the tensile coupon yield stress of the bottom chord was substituted for the top chord. Table 4.1 lists the tensile coupon data for the tests used in this study.

For the case where the top chord yields in compression at ultimate load, the initial top chord stress due to concrete placement is subtracted from the top chord yield stress in the model. This is the case for CLH-4 and CLH-11. For the case where the top chord yields in tension at ultimate load, the initial top chord stress is added to the top chord yield stress in the model. This is the case for CLH-9. For the case where the top chord does not yield in tension or compression, no adjustment needs to be made to the top chord yield strain. This was the case for CLH-5 through CLH-8.

The material behavior of the steel top and bottom chords is modeled using an idealized elastic-plastic stress-strain curve as shown in Figure 4.2. The bilinear behavior of the top and bottom chords were assumed to be the same in tension as in compression.

Table 4.1 Tensile Coupon Test Data

Test	Bot. Chord Coupon F_y (psi)	Bot. Chord Model F_y (psi)	Top Chord Coupon F_y (psi)	Top Chord Model F_y (psi)
CLH-4	62100	55000	55200	42100
CLH-5	59900	52700	59300	52400
CLH-6	56200	49500	56200[1]	46647
CLH-7	57100	51000	57100[1]	45500
CLH-8	56300	50700	56300[1]	65300
CLH-9	50400	37437	51270	66611
CLH-11	52700	46436	59100	48486

[1] Top chord tensile coupon data not available, bottom chord yield stress used

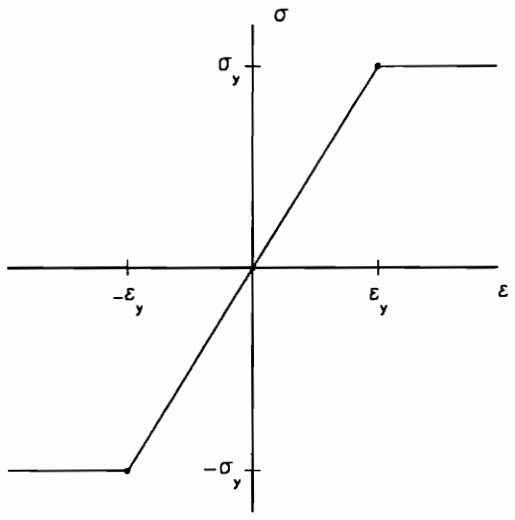

Figure 4.2 Idealized Elastic-Plastic Stress-Strain Curve

4.3.2 Steel Joist Webs

The steel joist web members were modeled as elastic elements. The webs were not modeled as plastic elements because for all the tests considered, the webs were overdesigned so that the bottom chord would yield before a web member failed. Consequently, the web members were modeled as elastic elements since it would require less modeling time and gave a sufficiently accurate model of the prototype behavior.

4.3.3 Steel Shear Studs

The shaft of the steel shear stud was assumed to be infinitely rigid, i.e., $I_{stud} > 1000$ times the largest moment of inertia for the composite joist member. The shear stiffness of the stud was modeled by using a two-node spring element at the base of the shear stud. The spring element connects the base of the shear stud to the top chord of the steel joist and its two nodes occupy the same point in space under no load. The stiffness of the spring element is modeled by the equation given by Ollgaard, et al. (1971) which was presented in a previous section of the report. This modeling technique is based on studies (Kitoh and Sonoda 1991) which show that the shear and axial force on the body of the stud is relatively small compared to the shear at the base of the stud. The study by Kitoh and Sonoda (1991) also found that the Ollgaard equation gave results that were closer to the measured forces and displacements on the stud than using an infinite stiffness at the stud base.

4.3.4 Concrete Slab

The concrete slab properties are transformed into equivalent steel properties by the modular ratio. The modular ratio is obtained by dividing the modulus of elasticity of the steel by the modulus of elasticity of the concrete. The modulus of elasticity of the concrete is calculated by the formula given in ACI 318-89:

$$E_C = 33(w_C)^{1.5}\sqrt{f'_C} \qquad (4.1)$$

where E_C = modulus of elasticity of concrete, psi

w_C = unit weight of concrete, pcf

f'_C = specified compressive strength of concrete, psi

The values of f'_C and w_C are given in Table 4.2.

Table 4.2 Values of f'_C and w_C

TEST	f'_C (psi)	w_C (pcf)
CLH-4	3110	145
CLH-5	5860	145
CLH-6	4430	145
CLH-7	5720	145
CLH-8	5380	145
CLH-9	3170	145
CLH-11	2904	110

The concrete was assumed not cracked and concrete crushing was assumed not to be the controlling mode of failure. Hence, these properties were not included in the finite element model. In addition, no yield point is specified for the concrete slab stress-strain curve.

4.4 Composite Joist Support Conditions

The composite joist tests simulate a simply supported structure that is symmetric about its centerline. The computation time can be reduced by modeling only half of the composite joist due to its symmetry both in loading conditions and boundary conditions. The support condition on the end of the joist consists of a horizontal roller. The support condition at the centerline of the joist consists of a fixed support with a vertical shear release. This centerline support would prevent any horizontal displacement or rotation, similar to the behavior of the real structure. The centerline support condition is applied to the concrete slab, the top chord, and the bottom chord.

4.5 Variation of the Finite Element Model Parameters

The parameters involved in the modeling process need to be varied and examined for their effects on the overall model response. This section will describe the parameters that were evaluated. The prototype chosen for experimental modeling was CLH-11. There is no particular reason for choosing CLH-11. Any of the other tests could have been substituted for this parameter study.

Various models were tried for the shear studs. The first model used an infinitely stiff stud model which would result in no slip between the top and bottom of the stud. The second model used the actual shear stud properties calculated from the stud diameter. The third model used an infinitely stiff beam element for the stud shank and a nonlinear spring element for the stud base. The fourth and fifth models were the same as the third model, except the ultimate shear capacity of the stud calculated from the AISC equation were varied. The most accurate model was then checked for mesh fineness.

4.5.1 Infinitely Stiff Shear Connector Model

As shown in Figure 4.3, the model using infinitely stiff shear connectors does not give an accurate representation of the prototype behavior. The model response is stiffer than the prototype response. The model also gives a much higher ultimate load than the prototype ultimate load.

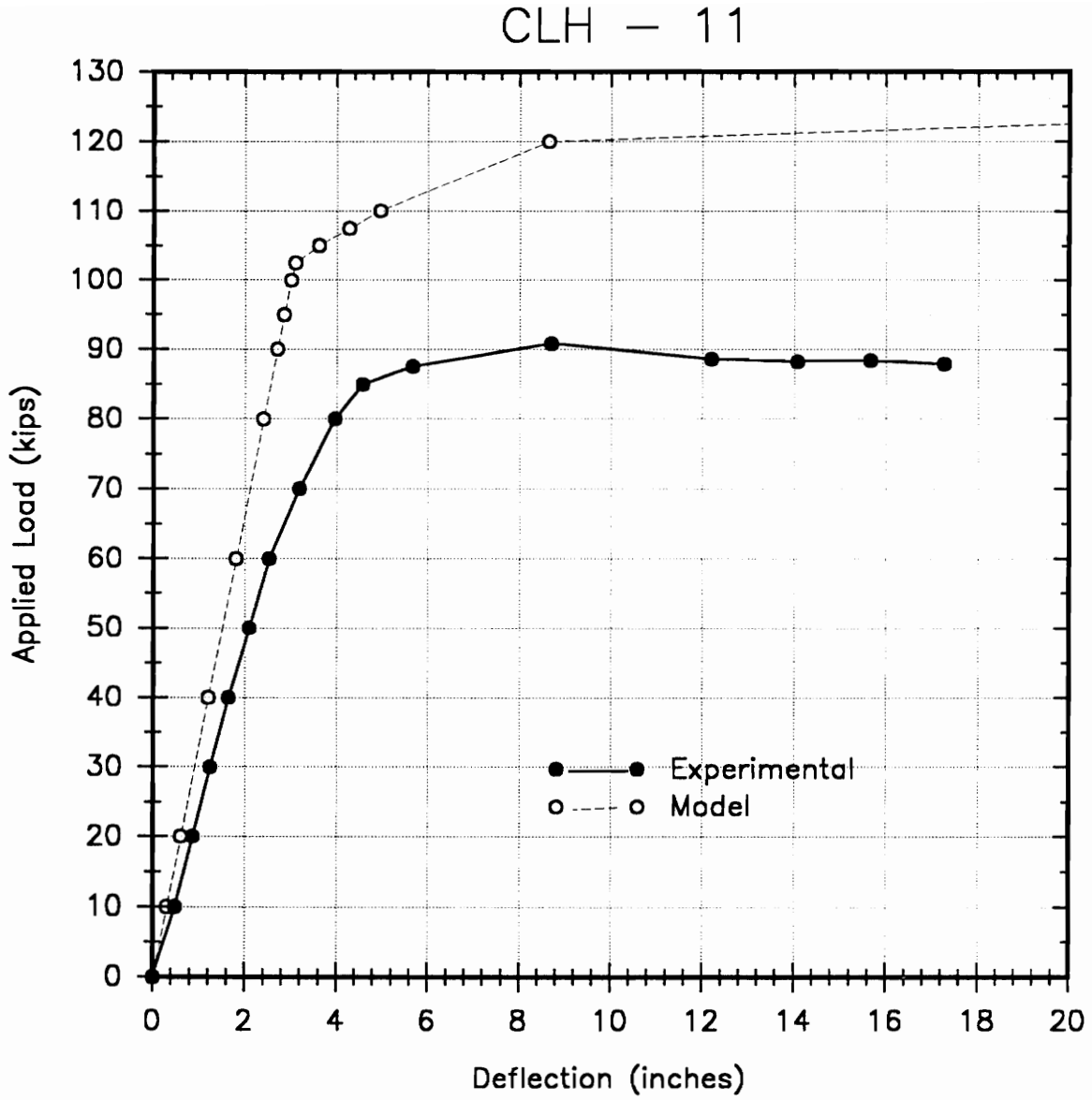

Figure 4.3 Applied Load vs. Centerline Deflection Using Infinite Shear Stud Stiffness

4.5.2 Model Using the Actual Shear Stud Properties

The area and moment of inertia of the 3/4" diameter shear studs in test CLH-11 were calculated and entered for the properties of the shear connector's shaft. The base of the stud is assumed infinitely rigid. This model is less stiff than the prototype and yields a lower ultimate load than the prototype as shown in Figure 4.4. The reason for this may be that the concrete slab acts as a concentrated force on the stud in the model whereas in reality the concrete acts as a distributed load on the shear stud. The concentrated force would give the same shear at the top of the stud as at the bottom of the stud. This is not a representation of the actual behavior according to Kitoh and Sonoda (1991). They report significantly more shear at the base of the stud than on the shaft of the stud at any location. This would be the case for the distributed load on the shear stud. Consequently, the stud deforms more in the model than in the actual test, resulting in a less stiff response. However, the ultimate load of the model is higher than the prototype ultimate load. Figure 4.5 shows the load vs. slip curves for the model and the prototype. The model endslip shows poor agreement with the prototype response. The model endslip seems to vary linearly with load whereas the prototype endslip seems to vary exponentially with load.

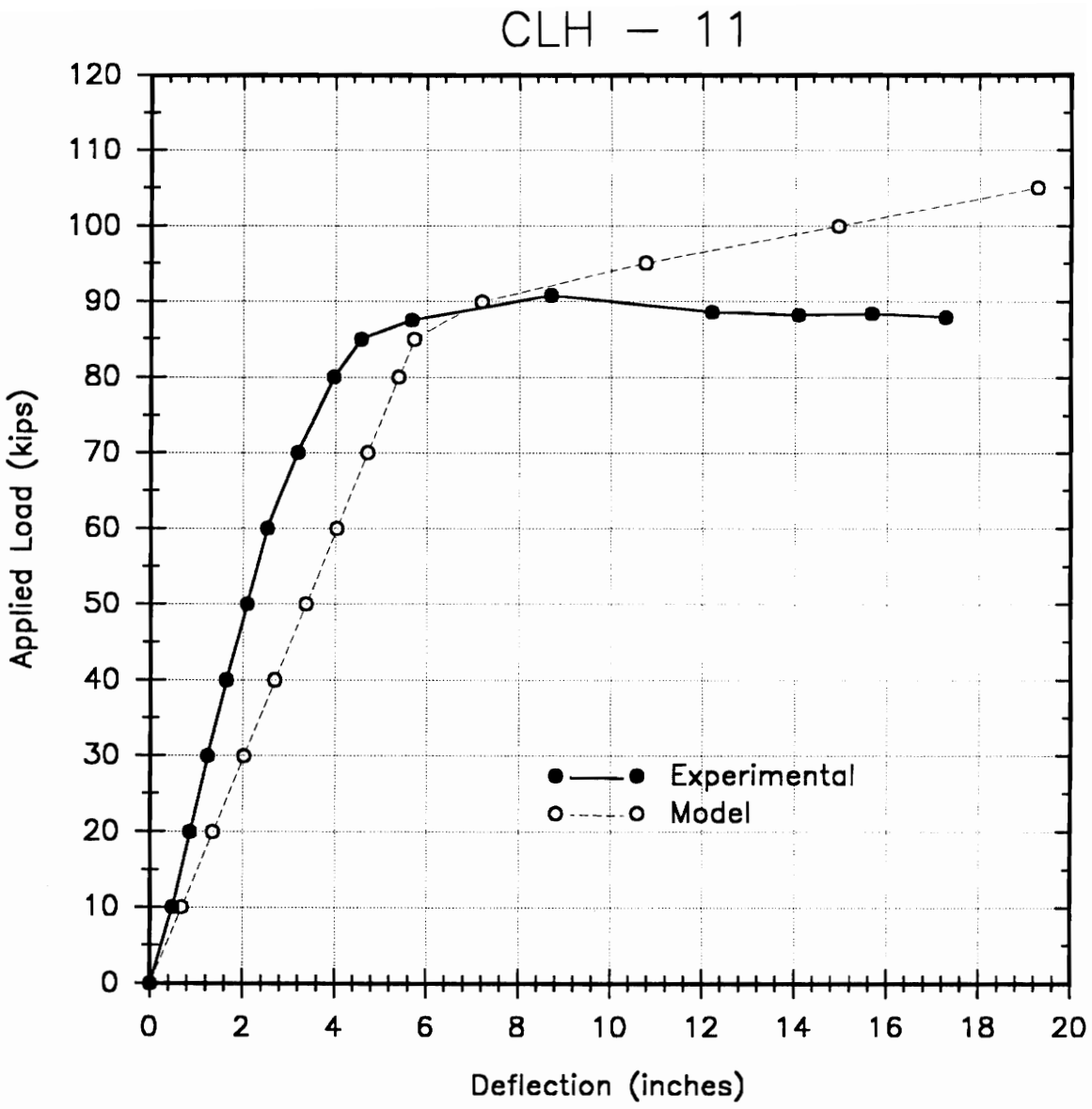

Figure 4.4 Applied Load vs. Centerline Deflection Using Actual Shear Stud Properties

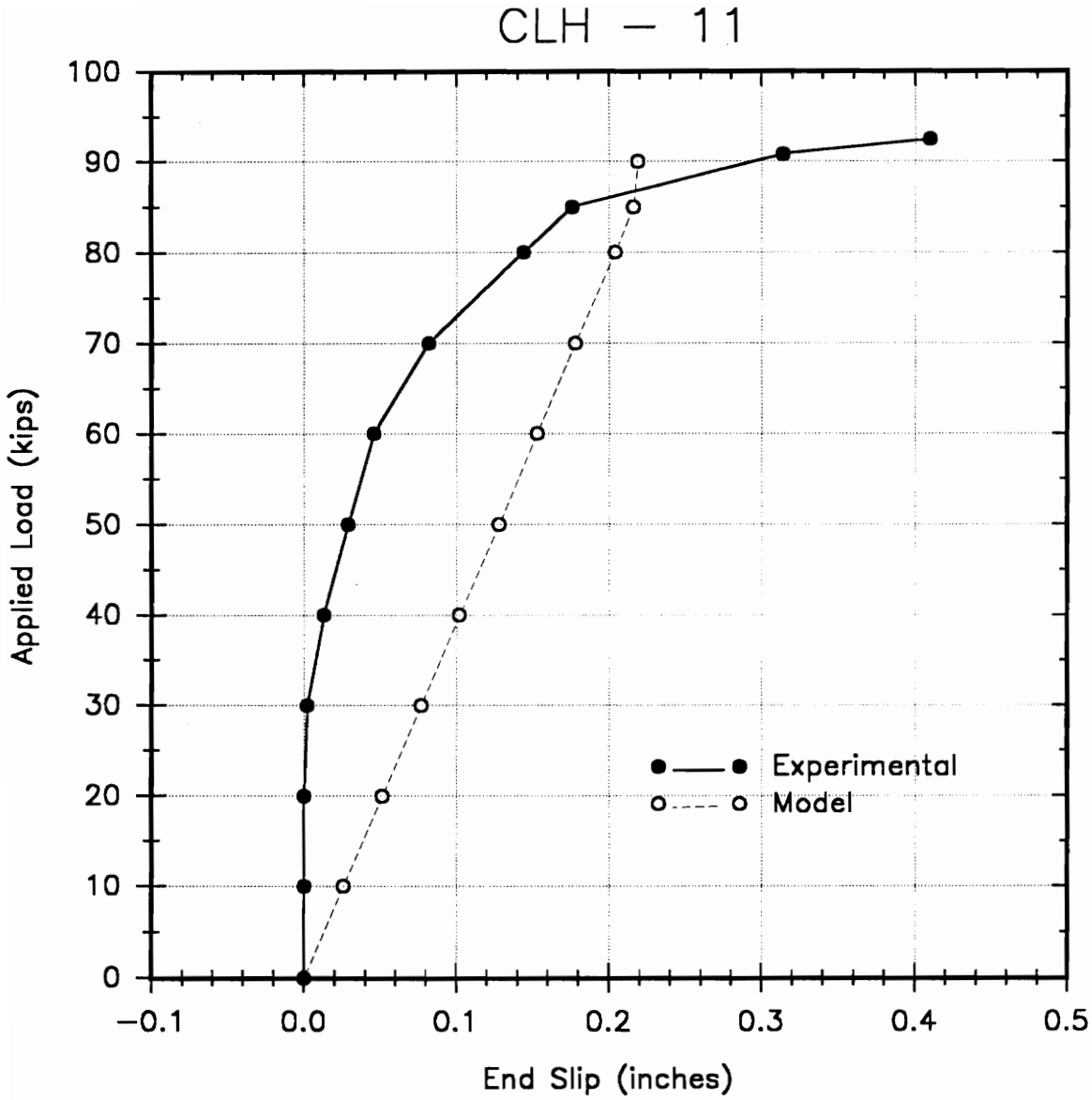

Figure 4.5 Applied Load vs. End Slip Using Actual Shear Stud Properties

4.5.3 Ollgaard Representation of the Stud Stiffness

Tests conducted by Ollgaard et al. (1971) showed that the shear force-deformation behavior of the shear studs used in the tests can be represented by Eq. (1.2) which is repeated here:

$$Q = Q_u(1-e^{-18x})^{2/3} \qquad (1.2)$$

A typical plot of the Ollgaard, et al. equation is shown in Figure 4.6.

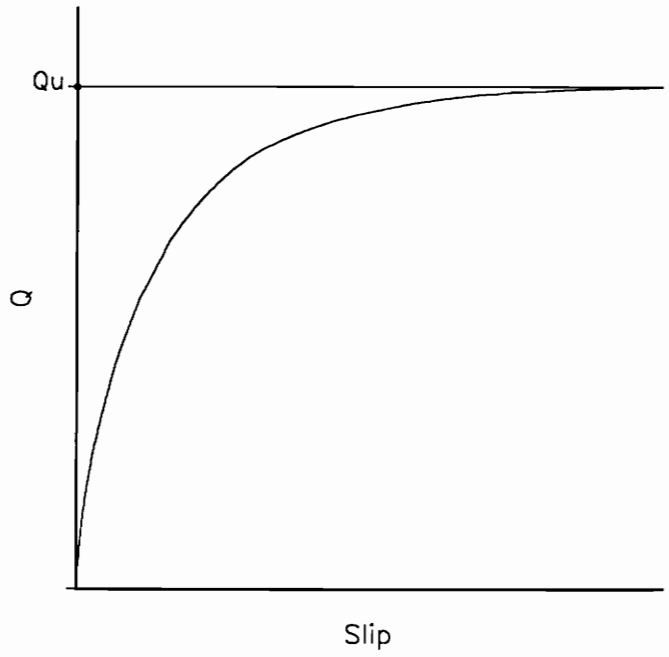

Figure 4.6 Plot of Ollgaard, et al. Equation

The ultimate shear capacity of the shear stud, Q_u, is calculated from the AISC equation (LRFD 1986):

$$Q_u = 0.5(A_{sc})(f'_c E_c)^{0.5} \leq A_{sc} F_u \quad (4.2)$$

where Q_u = ultimate shear capacity of the stud, kips

A_{sc} = cross-sectional area of the shear stud, in^2

f'_c = specified compressive strength of concrete, ksi

E_c = modulus of elasticity of the concrete, ksi

F_u = minimum specified tensile strength of stud, ksi

The results of using the Ollgaard, et al. equation with the ultimate shear capacity calculated directly from the AISC equation for the stud model is compared with the experimental result as shown in Figure 4.7. The shear force-slip curves of the model and prototype are given in Figure 4.8. The model endslip curve shows better agreement with the prototype behavior using the equation given by Ollgaard, et al. (1971).

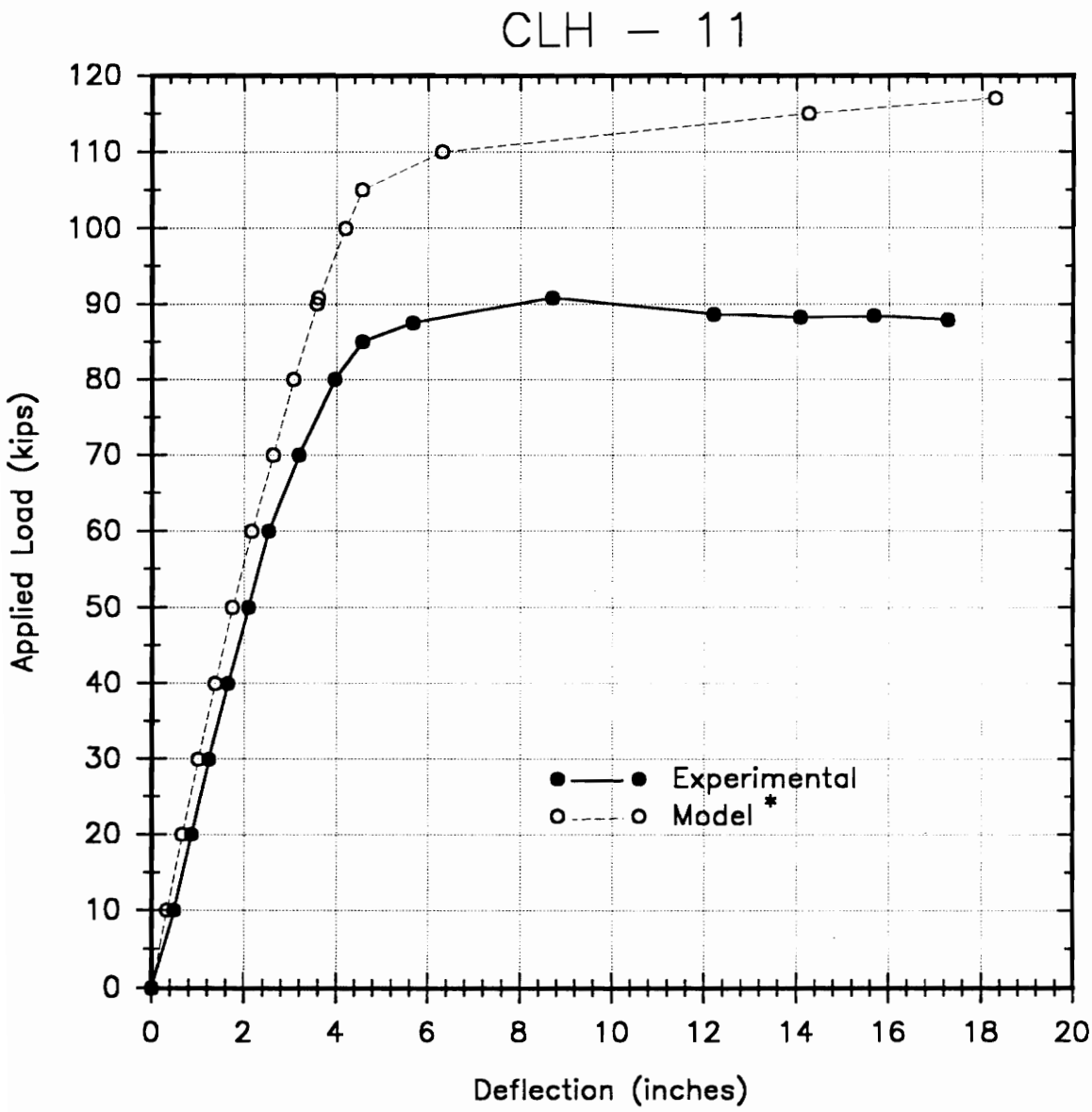

* Ultimate shear capacity of the studs was obtained directly from the AISC equation

Figure 4.7 Applied Load vs. Centerline Deflection Using Ollgaard Equation with No Factors on the AISC Equation

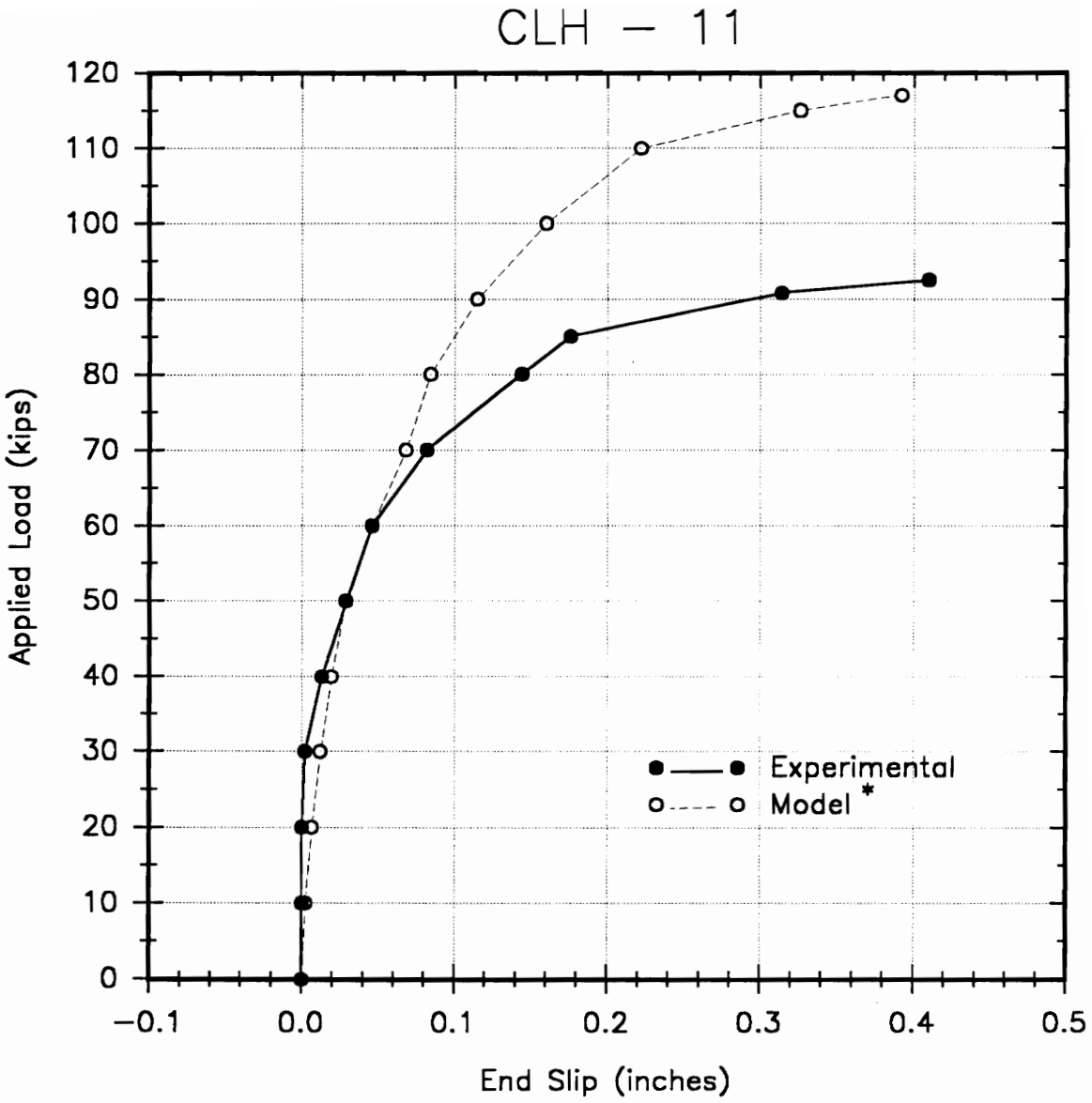

* Ultimate shear capacity of the studs was obtained directly from the AISC equation

Figure 4.8 Applied Load vs. End Slip Using Ollgaard Equation with No Factors on the AISC Equation

Push-off tests performed by Sublett (1991) show that the AISC equation is unconservative in predicting the actual ultimate capacity of the shear studs. The results of Sublett's tests indicate that the ultimate capacity of the studs in the strong position is approximately 65% of the calculated value using the AISC equation. Similarly, the ultimate capacity of the studs in the weak position is approximately 50% of the calculated value. Consequently, the model should account for this difference. The ultimate shear capacity obtained from Equation (4.2) is multiplied 0.65 for the strong position studs and 0.50 for the weak position studs.

For test CLH-11, the studs were alternated between strong and weak positions, so the strong and weak ultimate capacities were alternated between the shear studs in the model. The results of the model are shown in Figure 4.9 and Figure 4.10. The model using the modified AISC ultimate shear capacity for the studs shows a significantly improved comparison between the model and prototype stiffness and ultimate load capacity.

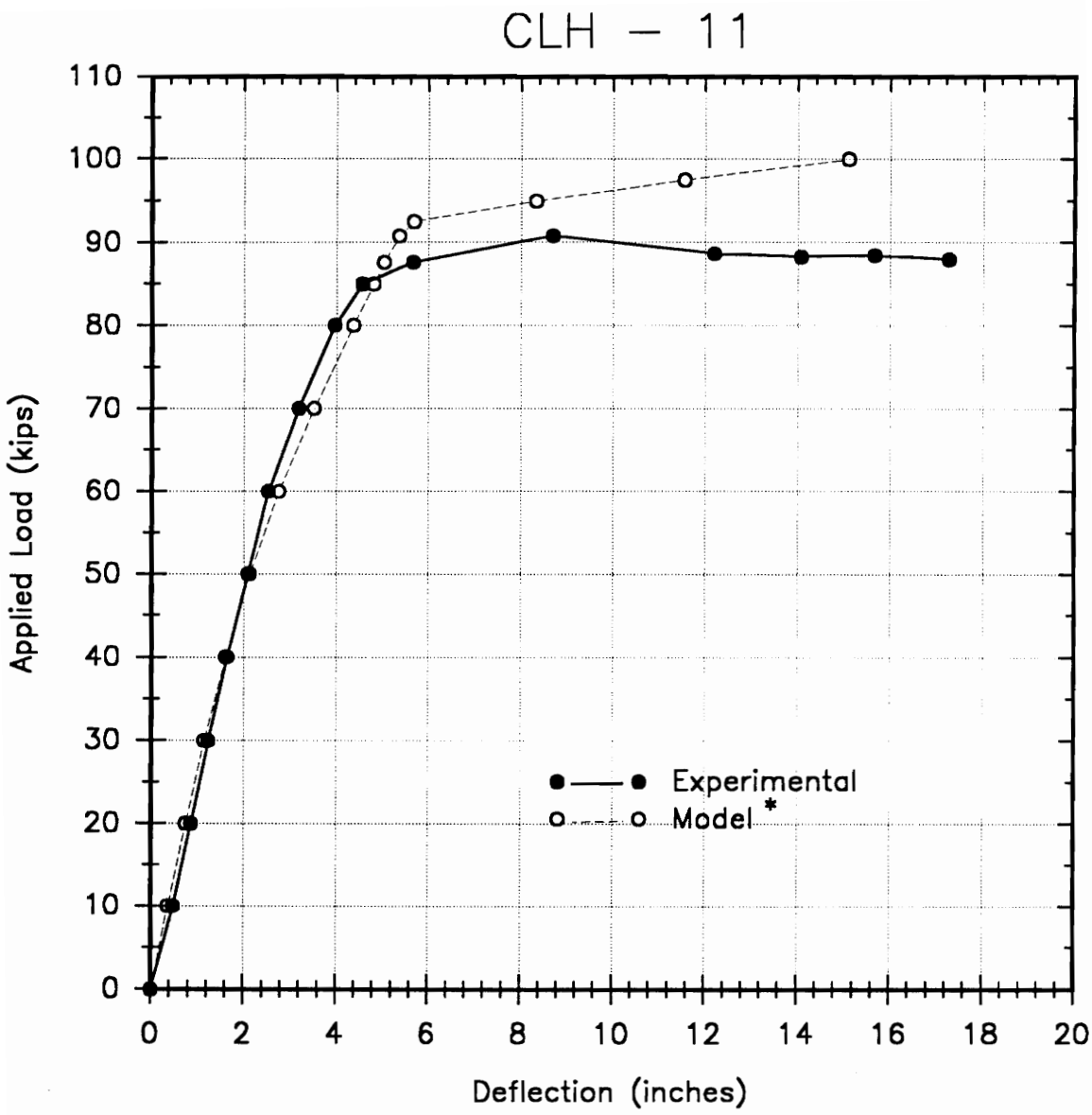

* This model uses 65% and 50% of the AISC ultimate shear capacity for the studs in the strong and weak position, respectively

Figure 4.9 Applied Load vs. Centerline Deflection Using Ollgaard Equation

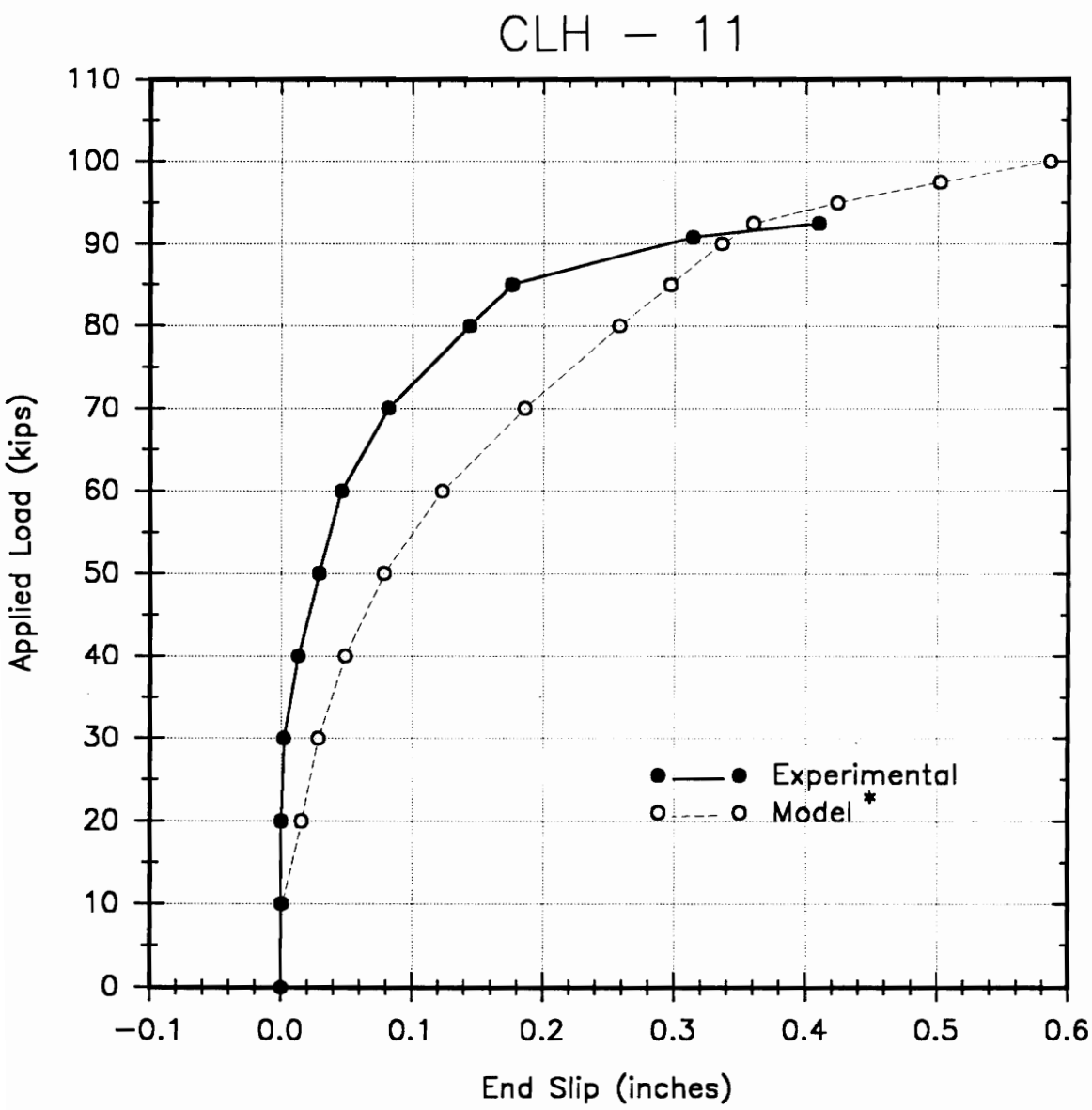

* This model uses 65% and 50% of the AISC ultimate shear capacity for the studs in the strong and weak position, respectively

Figure 4.10 Applied Load vs. End Slip Using Ollgaard Equation

To see the importance of correctly modeling the behavior of the studs, the stiffness values obtained from the previous discussion can be varied to see the effect it has on the overall composite joist model performance. The stud stiffnesses were multiplied by factors of 0.5, 1.0, and 2.0. The applied load vs. composite joist deflection curves are shown in Figure 4.11. The load vs. deflection plot shows that the factor of 1.0 gives the best representation of the prototype stiffness and ultimate capacity. Figure 4.12 shows the applied load vs. the end slip. Again, the factor of 1.0 gives the best representation of the stiffness and ultimate capacity.

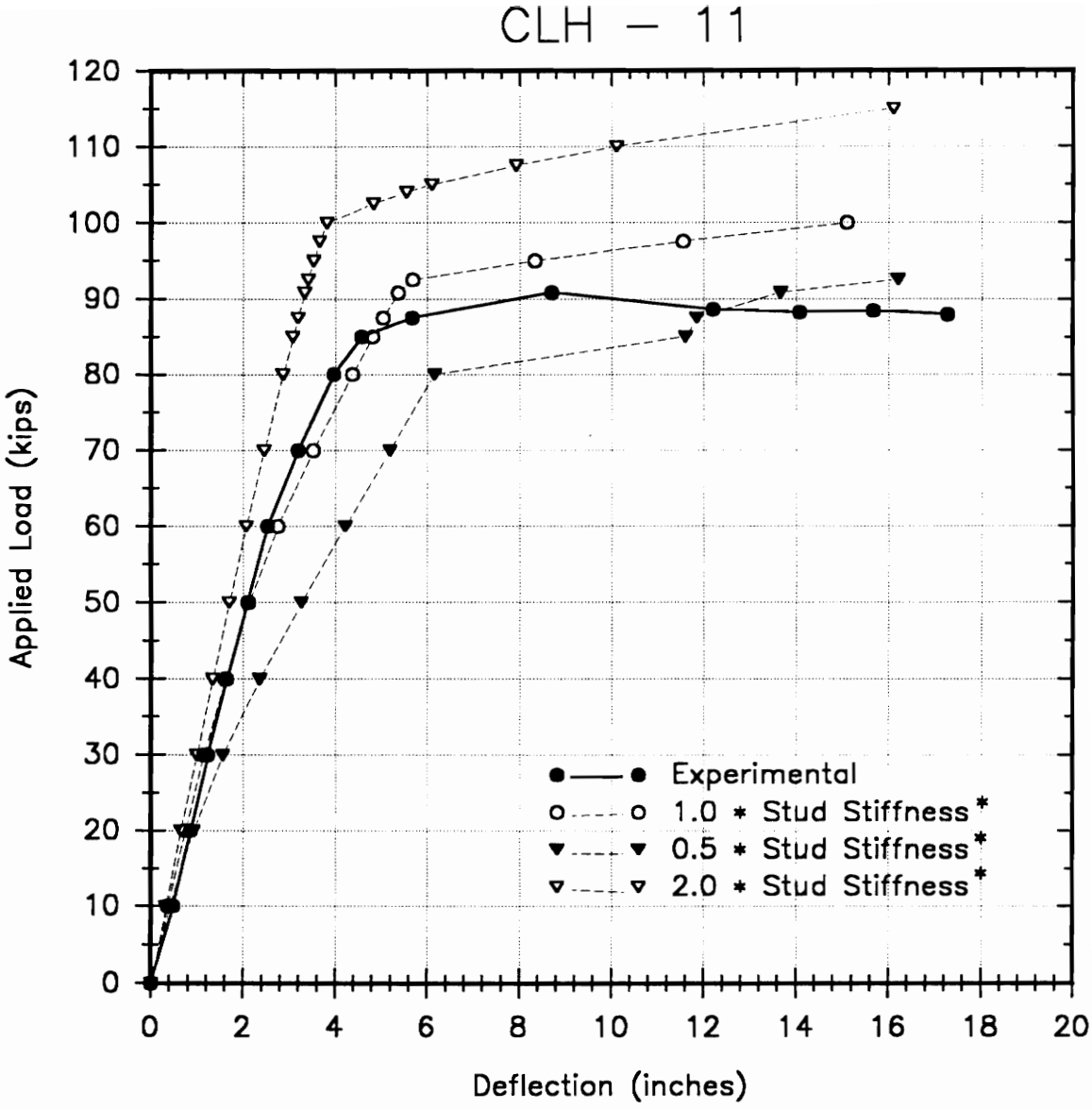

* This model uses the Ollgaard equation for the stud stiffness and 65% and 50% of the AISC ultimate shear capacity for the strong and weak studs, respectively

Figure 4.11 Applied Load vs. Centerline Deflection for Varying Stud Stiffnesses

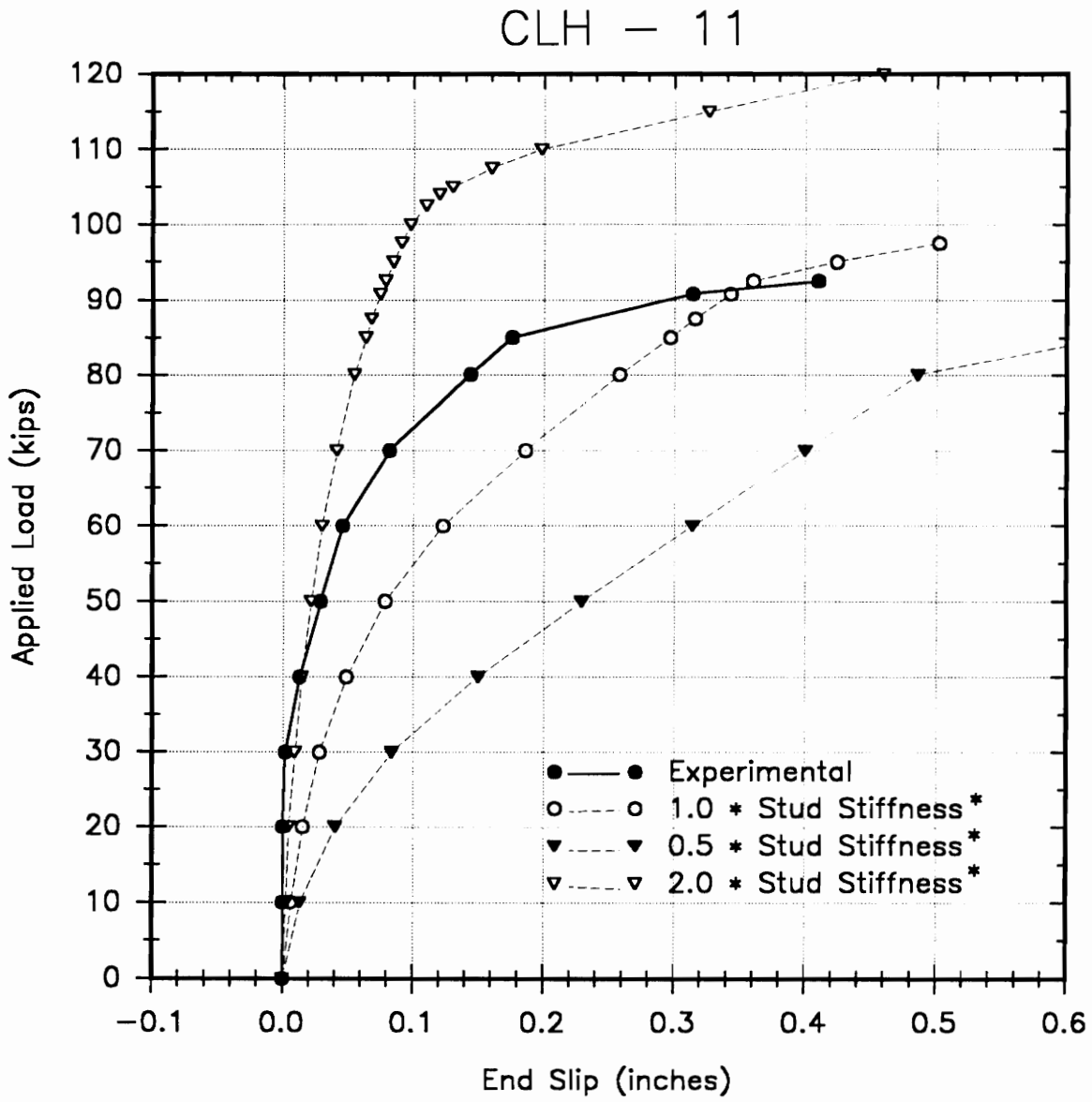

* This model uses the Ollgaard equation for the stud stiffness and 65% and 50% of the AISC ultimate shear capacity for the strong and weak studs, respectively

Figure 4.12 Applied Load vs. End Slip for Varying Stud Stiffnesses

4.5.4 Mesh Fineness

To ensure convergence of the model, mesh fineness tests need to be performed. Model 1 has elements generated between panel points. Model 2 is twice as fine as Model 1. Model 3 has the same fineness as Model 1 except that the top chord and bottom chord are twice as fine as that of Model 1.

4.5.4.1 Model 1

Model 1 has elements generated between panel points in the composite joist. This is the simplest model to generate. The response of this model using the Ollgaard equation and the modified AISC ultimate shear capacity for the stud stiffness is shown in Figure 4.9 and Figure 4.10. Figure 4.13 shows the nodes which define the elements of the mesh.

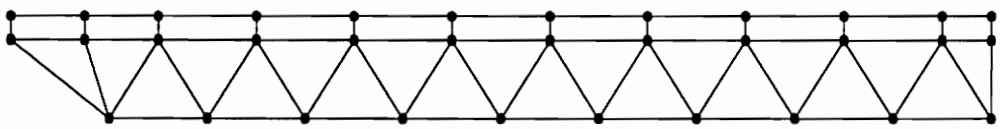

Figure 4.13 FE Mesh for Model 1

4.5.4.2 Model 2

Model 2 is the same as Model 1 in all respects except that the elements are twice as fine in Model 2. The element mesh fineness is shown

in Figure 4.14. The results of Model 2 are shown in Figure 4.15 and Figure 4.16. As the plots show, Model 2 is stiffer than the prototype response.

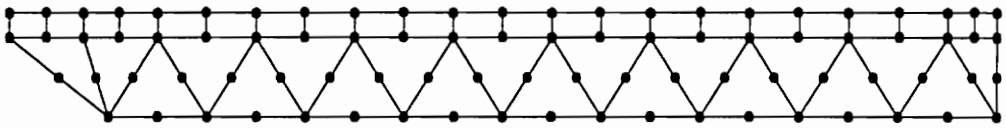

Figure 4.14 FE Mesh for Model 2

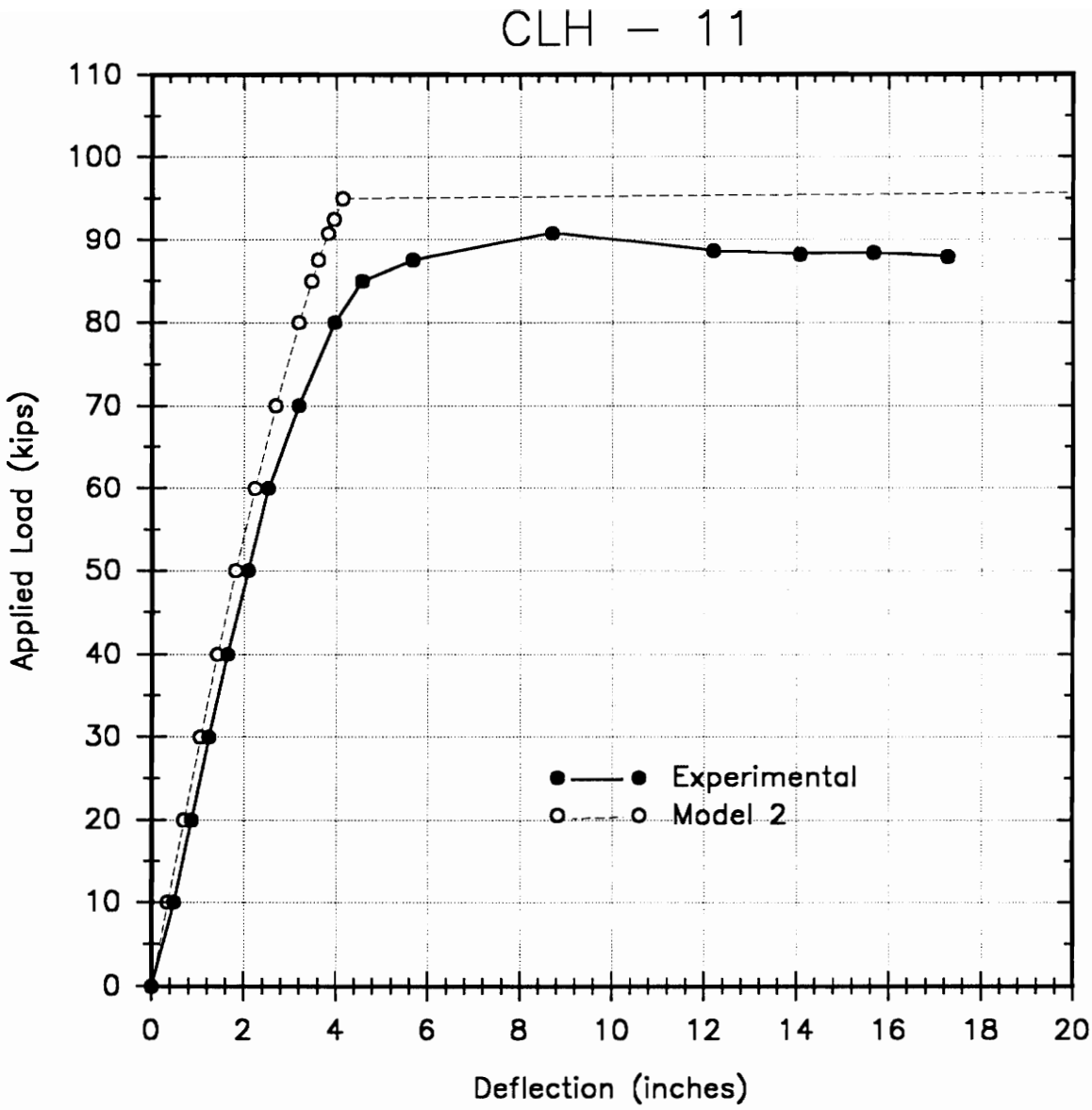

Figure 4.15 Applied Load vs. Centerline Deflection for Model 2

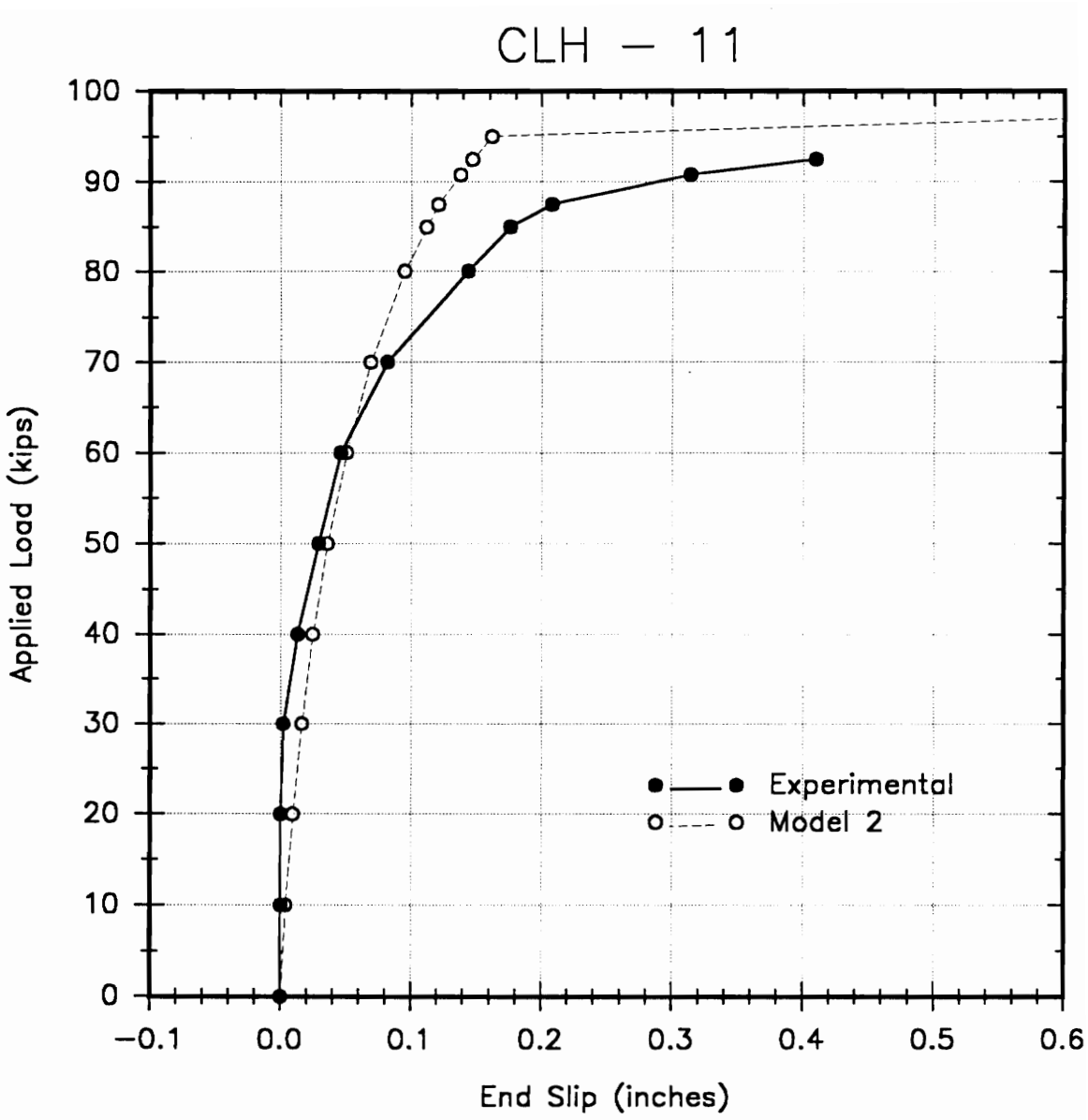

Figure 4.16 Applied Load vs. End Slip for Model 2

4.5.4.3 Model 3

Model 3 is the same as Model 1 in all respects except that the top and bottom chords are twice as fine as that of Model 1. Only the top and bottom chords were refined since these are the regions of high plasticity in the model. Figure 4.17 shows the mesh fineness of the top and bottom chords in the model. The results of Model 3 are compared to the experimental results in Figure 4.18 and Figure 4.19.

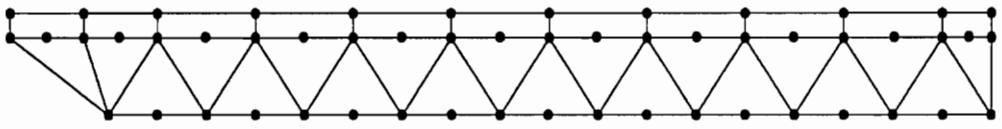

Figure 4.17 FE Mesh for Model 3

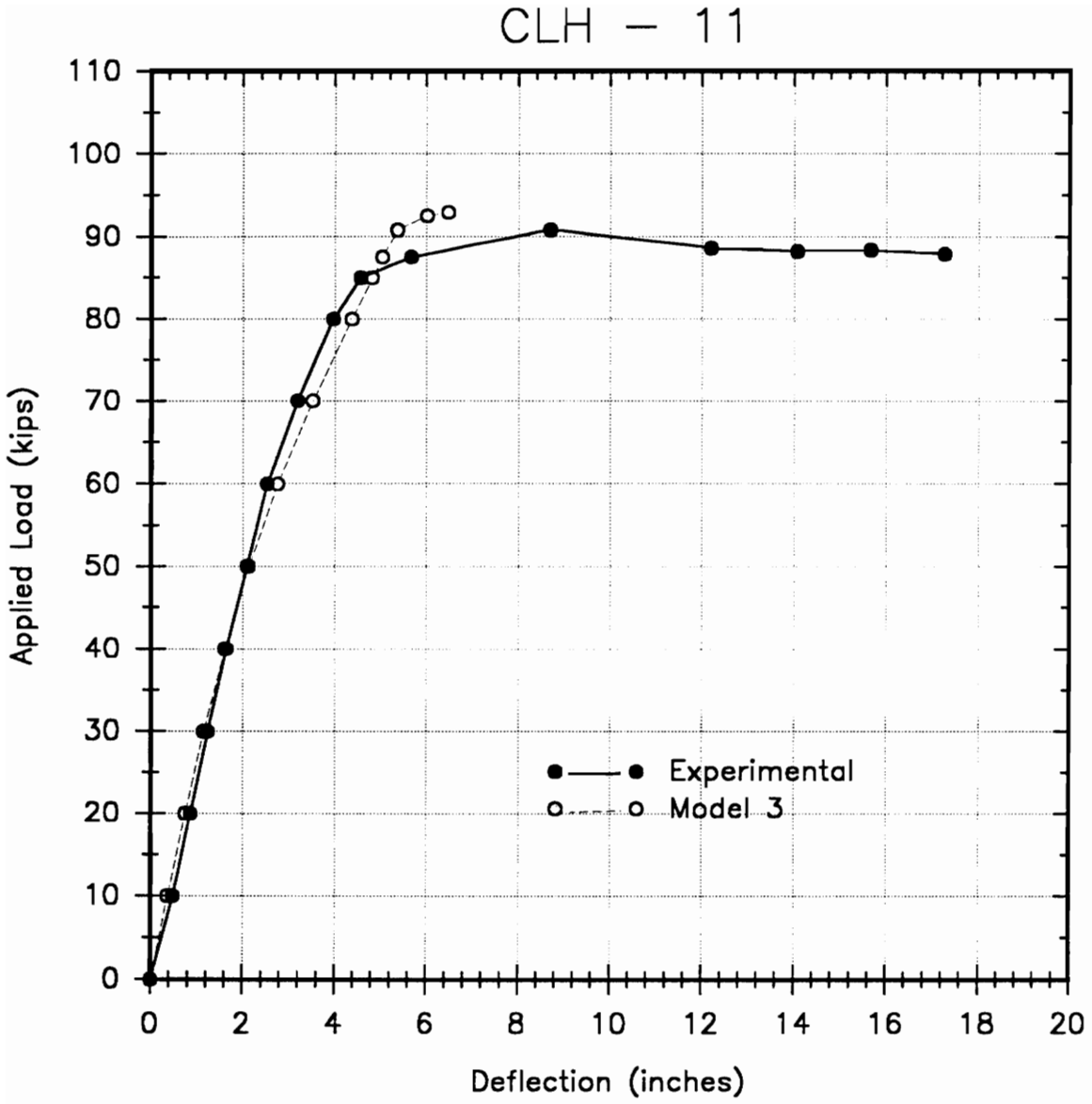

Figure 4.18 Applied Load vs. Centerline Deflection for Model 3

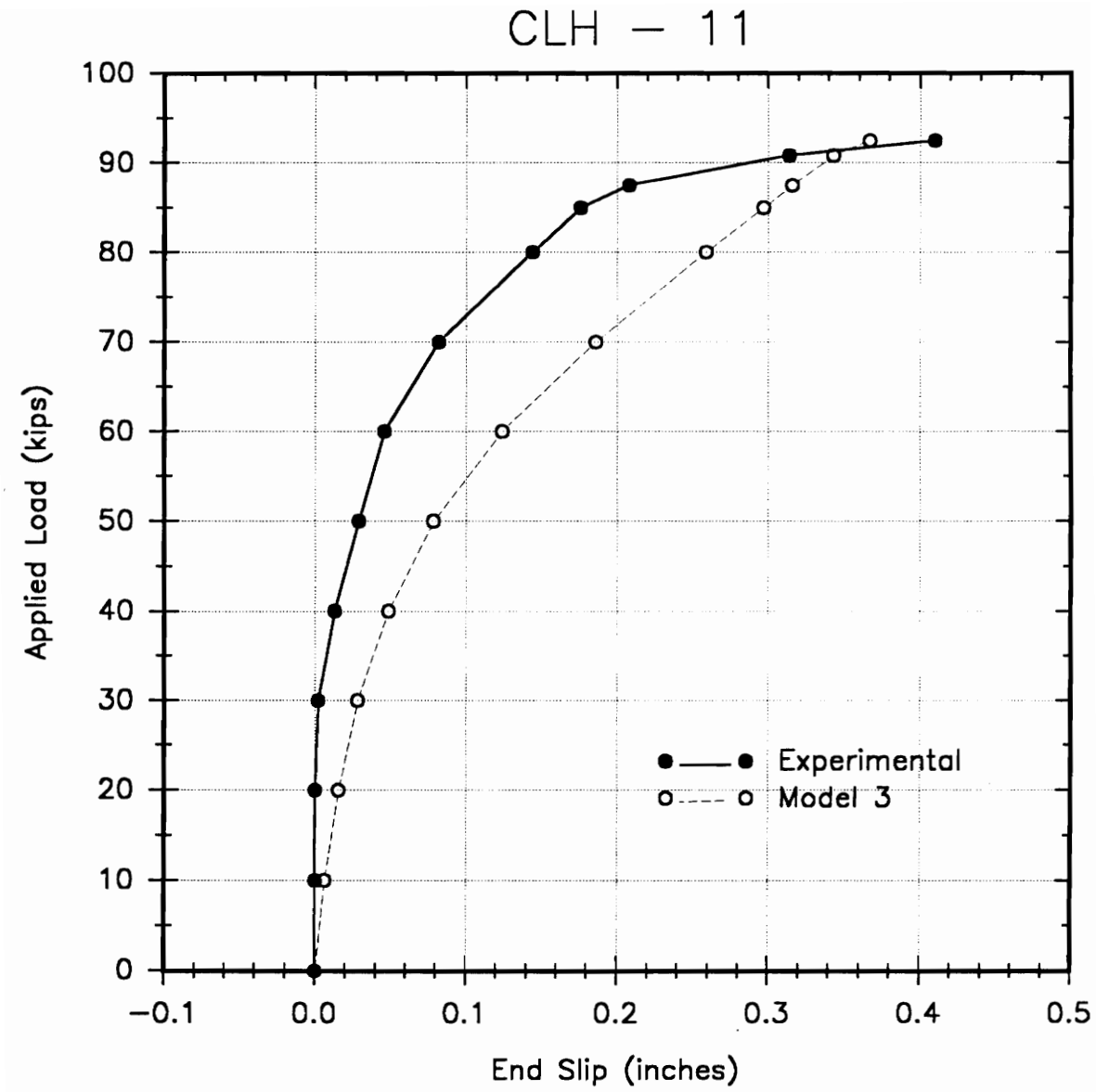

Figure 4.19 Applied Load vs. End Slip for Model 3

4.5.4.4 Summary of Models

The plots of Model 1, Model 2, and Model 3 show revealing results. Model 2 is stiffer than Model 1, Model 3, and the prototype. Model 1 gives the best representation of the prototype response and further mesh refinement is shown to be unnecessary for this study.

In summary, the best model representation of the prototype uses the Ollgaard equation to describe the shear deformation of the studs. The AISC ultimate shear capacity equation needs to factored by 0.65 for the strong position studs and 0.50 for the weak position studs. Finally, generating elements between the panel points of the composite joist gives sufficient accuracy of the prototype response.

4.6 Tests for Nonlinear Convergence

There are no set guidelines to assure convergence of the nonlinear behavior of a structure. The widely accepted procedure for modeling the nonlinear behavior of a structure is to apply a load near the yield load of the structure and increment the load by 5% to 10% of the yield load (Wegmuller 1977; Swanson 1989a). The ANSYS Theoretical Manual (Swanson 1989a) also suggests using the larger of $(E_T/E)P_y$ or $0.05P_y$ where E_T is the tangent modulus, E is the modulus of elasticity, and P_y is the yield load. Since the tangent modulus is zero for the joist, $0.05P_y$ was used for the load increments of the models.

Another question posed in the nonlinear analysis of a structure is the number of iterations required for the results to converge within a specified

error tolerance. Since there are two nonlinearities in this model, the iterations required for the nonlinear stud shear force-slip curve and the plastic top and bottom chords of the steel joist must be tested separately.

4.6.1 Convergence Test for the Nonlinear Shear Stud

The nonlinear shear stud was isolated and modeled with the same boundary conditions as found in the composite joist model. The location of the spring element nodes on the stud is shown in Figure 4.20. Figure 4.21 shows the isolated model of the shear stud. The nonlinear model showed that convergence of the nonlinear stud response can be attained within a maximum of eleven iterations.

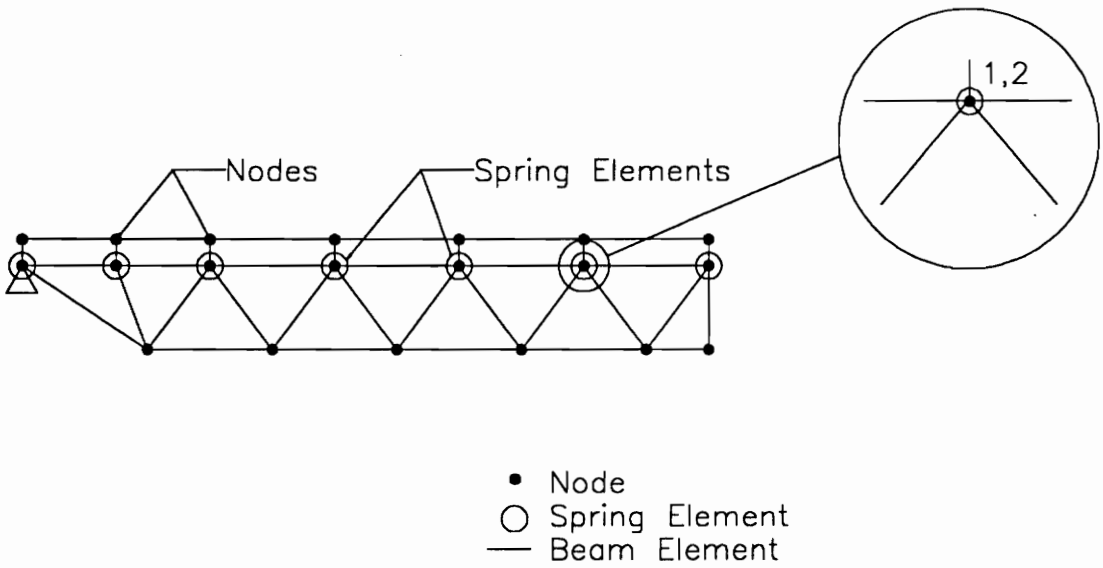

Figure 4.20 Spring Element Nodes

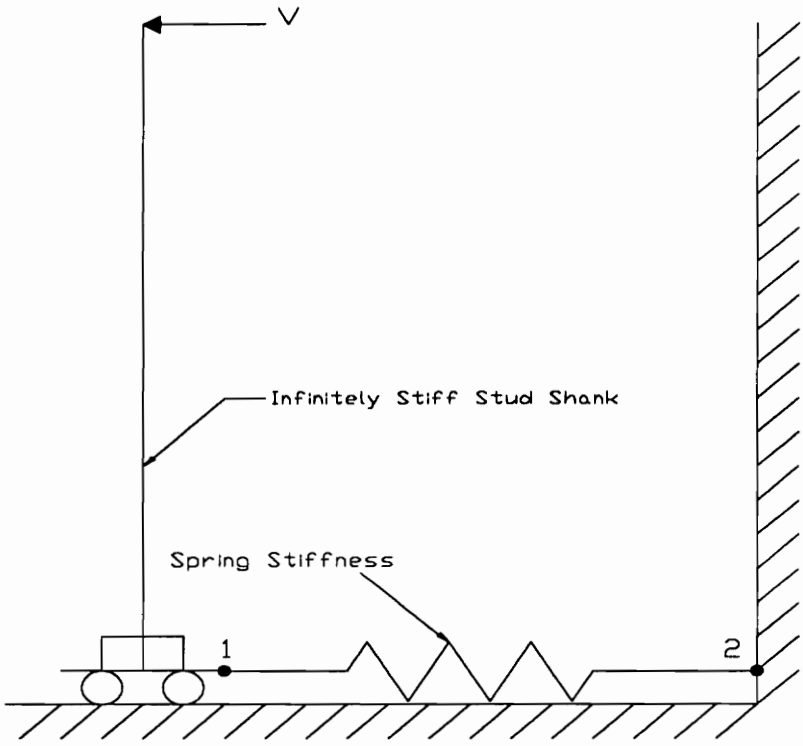

Figure 4.21 Shear Stud Model

4.6.2 Convergence Test for a Plastic Beam

The convergence requirement for the plastic top and bottom chords of the steel joist can be determined by modeling the behavior of an elastic-plastic plastic beam. The simply supported plastic beam model is shown in Figure 4.22. The idealized elastic-plastic stress-strain curve of the beam is shown in Figure 4.2. The number of iterations required for convergence at the yield load is three. Using the results of this model and the shear stud model, the number of iterations required for convergence of the composite joist model should be no greater than the higher of the two iterations, or

eleven. For this study, fifteen iterations were used in the nonlinear analysis of the composite joist.

In addition, the following plasticity convergence criterion was used (Swanson 1989a):

$$\Delta\varepsilon^{pl}/\varepsilon^{el} \leq \gamma \qquad (4.3)$$

where $\Delta\varepsilon^{pl}$ = additional plastic strain calculated for the current iteration

ε^{el} = elastic strain of current iteration

γ = preset error tolerance

A plastic convergence criterion of 0.5 was used for the elastic-plastic region to satisfy equilibrium. The plastic convergence criterion was relaxed to about 1.0 in the plastic region.

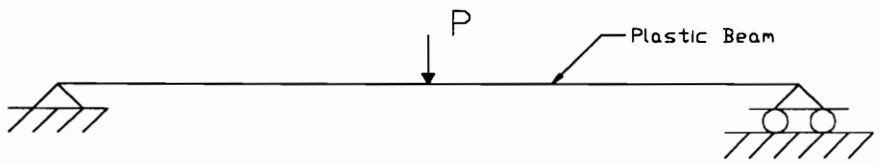

Figure 4.22 Elastic-Plastic Beam Model

CHAPTER V

FINITE ELEMENT MODELS OF COMPOSITE JOISTS

5.1 FE Model of Composite Joist CLH-4

Composite joist CLH-4 had 22 shear studs per half span in the prototype which were proportioned to 9 shear connectors in the model. The shear studs were all modeled as being in the weak position. See Figure 3.4 for the stud positions. The steel joist out-to-out depth was 16 in. The joist depth from the neutral axis of the top chord to the neutral axis of the bottom chord was modeled as 13.6 in. Figure 5.1 shows the model layout. The member properties of the finite element model are given in Table 5.1.

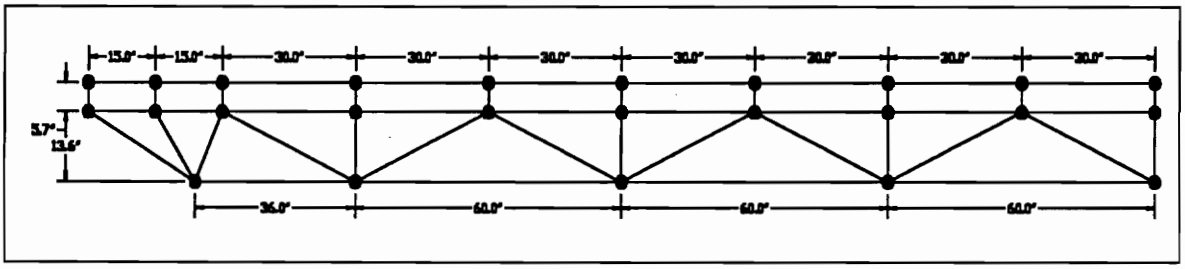

Figure 5.1 FE Mesh Layout for Model CLH-4

Table 5.1 Member Properties for CLH-4

MEMBER	AREA (in^2)	I (in^4)
CONCRETE SLAB	26.9	20.2
W2	2.875	2.488
W3	1.634	0.615
W4	2.621	2.284
W5	2.875	2.448
W6	1.810	1.276
W7	2.031	1.218
W8	0.962	0.202
W9	1.036	0.304
W10	0.882	0.188
2DL	0.206	0.019
TOP CHORD	4.186	4.904
BOTTOM CHORD	8.376	20.062
V2, V3	0.206	0.019
V4, V5	1.000	0.0833

5.2 FE Model of Composite Joist CLH-5

Composite joist CLH-5 had 11 shear studs per half span in the prototype which were proportioned to 8 shear connectors in the model. The shear studs were all modeled as being in the strong position. See Figure 3.4 for the stud positions. The steel joist out-to-out depth was 34 in. The joist depth from the neutral axis of the top chord to the neutral axis of the bottom chord was modeled as 32.0 in. Figure 5.2 shows the model layout. The member properties of the finite element model are given in Table 5.2.

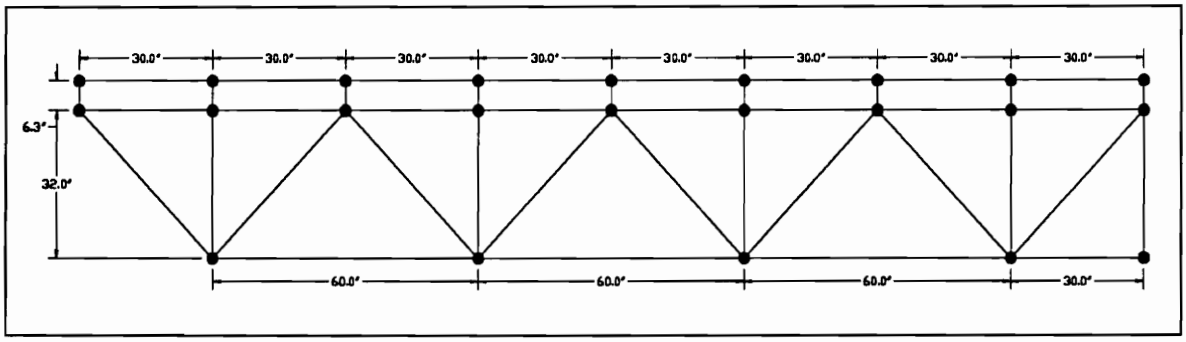

Figure 5.2 FE Mesh Layout for Model CLH-5

Table 5.2 Member Properties for CLH-5

MEMBER	AREA (in^2)	I (in^4)
CONCRETE SLAB	37.0	27.7
W2	1.876	0.696
W3	2.030	1.218
W4	1.426	0.544
W5	1.426	0.544
W6	0.962	0.202
W7	1.634	0.616
W8	0.481	0.101
W9	0.778	0.294
TOP CHORD	4.186	4.904
BOTTOM CHORD	4.186	4.904
V2, V3, V4, V5	0.518	0.152

5.3 FE Model of Composite Joist CLH-6

Composite joist CLH-6 had 18 shear studs per half span in the prototype which were proportioned to 8 shear connectors in the model. The shear studs were all modeled as being in the strong position. See Figure 3.4 for the stud positions. The steel joist out-to-out depth was 14 in. The joist depth from the neutral axis of the top chord to the neutral axis of the bottom chord was modeled as 12.0 in. Figure 5.3 shows the model layout. The member properties of the finite element model are given in Table 5.3.

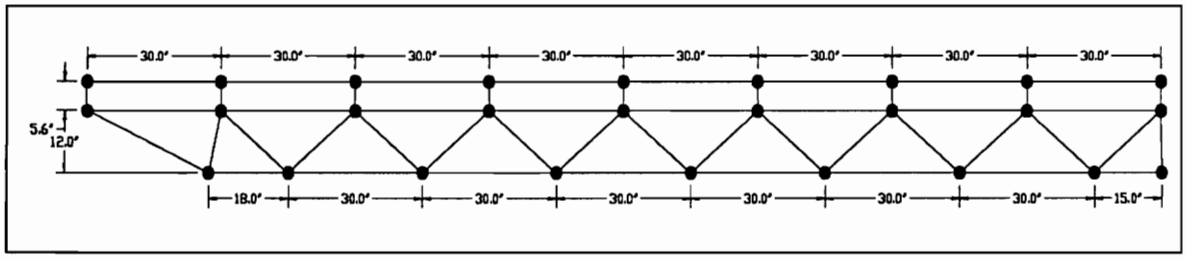

Figure 5.3 FE Mesh Layout for Model CLH-6

Table 5.3 Member Properties for CLH-6

MEMBER	AREA (in^2)	I (in^4)
CONCRETE SLAB	32.1	24.1
W2	3.560	3.024
W3	1.876	0.696
W4	1.876	0.696
W5	1.876	0.696
W6	1.876	0.696
W7	1.876	0.696
W8	1.250	0.482
W9	1.250	0.482
W10	0.962	0.202
W11	1.250	0.482
W12	0.630	0.092
W13	0.630	0.092
W14	0.630	0.092
W15	0.630	0.092
W16	0.630	0.092
W17	0.630	0.092
TOP CHORD	3.560	3.024
BOTTOM CHORD	6.624	9.958

5.4 FE Model of Composite Joist CLH-7

Composite joist CLH-7 had 18 shear studs per half span in the prototype which were proportioned to 8 shear connectors in the model. The shear studs were all modeled as being in the strong position. See Figure 3.4 for the stud positions. The steel joist out-to-out depth was 20 in. The joist depth from the neutral axis of the top chord to the neutral axis of the bottom chord was modeled as 18.0 in. Figure 5.4 shows the model layout. The member properties of the finite element model are given in Table 5.4.

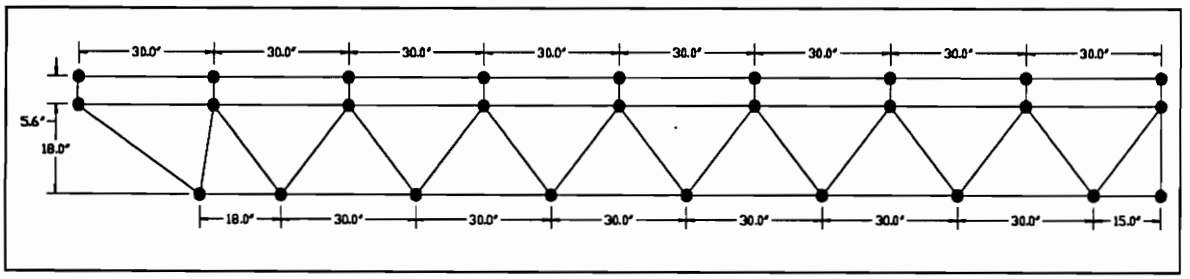

Figure 5.4 FE Mesh Layout for Model CLH-7

Table 5.4 Member Properties for CLH-7

MEMBER	AREA (in^2)	I (in^4)
CONCRETE SLAB	36.6	27.5
W2	3.560	3.024
W3	1.876	0.696
W4	1.876	0.696
W5	1.876	0.696
W6	1.876	0.696
W7	1.876	0.696
W8	1.876	0.696
W9	1.876	0.696
W10	1.426	0.544
W11	1.876	0.696
W12	0.630	0.092
W13	0.708	0.154
W14	0.630	0.092
W15	0.708	0.154
W16	0.630	0.092
W17	0.708	0.154
TOP CHORD	3.560	3.024
BOTTOM CHORD	6.624	9.958

5.5 FE Model of Composite Joist CLH-8

Composite joist CLH-8 had 18 shear studs per half span in the prototype which were proportioned to 8 shear connectors in the model. The shear studs were all modeled as being in the strong position. See Figure 3.4 for the stud positions. The steel joist out-to-out depth was 20 in. The joist depth from the neutral axis of the top chord to the neutral axis of the bottom chord was modeled as 18.0 in. Figure 5.5 shows the model layout. The member properties of the finite element model are given in Table 5.5.

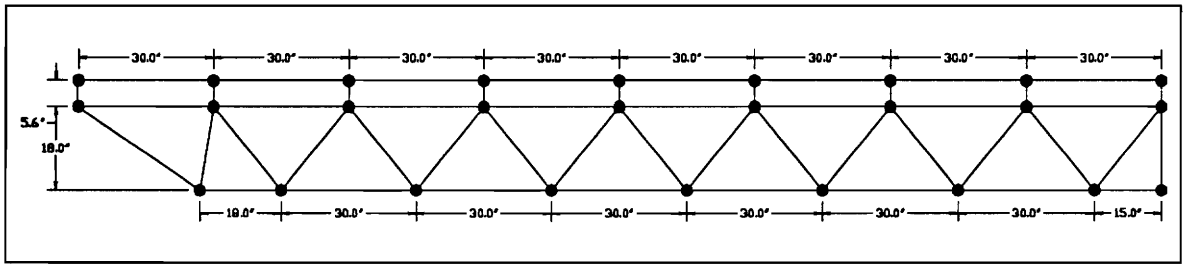

Figure 5.5 FE Mesh Layout for Model CLH-8

Table 5.5 Member Properties for CLH-8

MEMBER	AREA (in^2)	I (in^4)
CONCRETE SLAB	35.4	26.6
W2	2.376	1.406
W3	1.426	0.544
W4	1.250	0.482
W5	1.426	0.544
W6	1.250	0.482
W7	1.426	0.544
W8	0.882	0.188
W9	1.036	0.304
W10	0.818	0.174
W11	0.962	0.202
W12	0.522	0.078
W13	0.630	0.092
W14	0.412	0.038
W15	0.522	0.078
W16	0.412	0.038
W17	0.522	0.078
TOP CHORD	3.560	3.024
BOTTOM CHORD	6.624	9.958

5.6 FE Model of Composite Joist CLH-9

Composite joist CLH-9 had 11 shear studs per half span in the prototype which were proportioned to 9 shear connectors in the model. The shear studs were modeled as alternating between strong and weak positions. See Figure 3.4 for the stud positions. The steel joist out-to-out depth was 32 in. The joist depth from the neutral axis of the top chord to the neutral axis of the bottom chord was modeled as 30.3 in. Figure 5.6 shows the model layout. The member properties of the finite element model are given in Table 5.6.

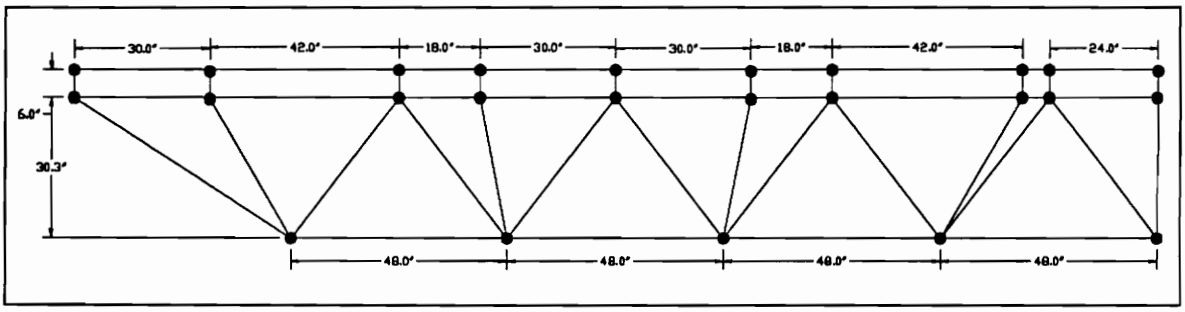

Figure 5.6 FE Mesh Layout for Model CLH-9

Table 5.6 Member Properties for CLH-9

MEMBER	AREA (in^2)	I (in^4)
CONCRETE SLAB	35.3	47.0
W2	3.214	2.756
W3	1.875	0.696
W4	1.875	0.696
W5	1.250	0.482
W6	0.882	0.188
W7	0.708	0.154
W8	0.630	0.092
W9	0.708	0.154
W10	0.630	0.092
2DL	0.713	0.272
TOP CHORD	3.560	3.024
BOTTOM CHORD	3.560	3.024

5.7 FE Model of Composite Joist CLH-11

Composite joist CLH-11 had 20 shear studs per half span in the prototype which were proportioned to 11 shear connectors in the model. The shear studs were modeled as alternating between strong and weak positions. See Figure 3.4 for the stud positions. The steel joist out-to-out depth was 16 in. The joist depth from the neutral axis of the top chord to the neutral axis of the bottom chord was modeled as 14.0 in. Figure 5.7 shows the model layout. The member properties of the finite element model are given in Table 5.7.

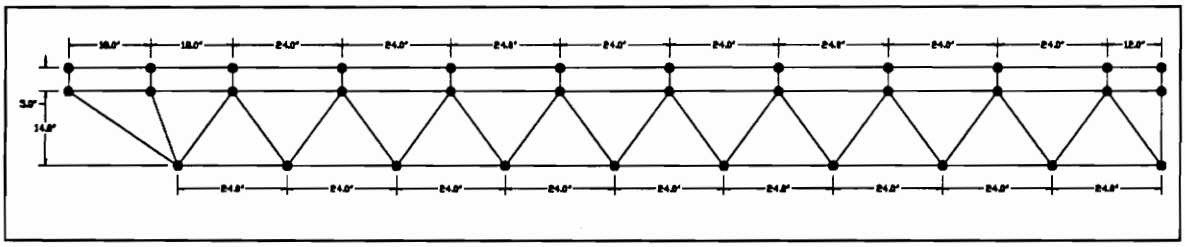

Figure 5.7 FE Mesh Layout for Model CLH-11

Table 5.7 Member Properties for CLH-11

MEMBER	AREA (in^2)	I (in^4)
CONCRETE SLAB	17.7	13.3
W2	2.376	1.406
W3	1.749	0.654
W4	1.426	0.544
W5	1.749	0.654
W6	1.426	0.544
W7	1.749	0.654
W8	0.790	0.170
W9	0.882	0.188
W10	0.708	0.154
W11	1.426	0.544
W12	0.630	0.092
W13	0.708	0.154
W14	0.481	0.101
W15	0.481	0.101
W16	0.566	0.165
W17	0.566	0.165
W18	0.481	0.101
W19	0.481	0.101
W20	0.481	0.101
2DL	0.409	0.087
TOP CHORD	3.560	3.024
BOTTOM CHORD	6.624	9.958

CHAPTER VI

RESULTS OF COMPOSITE JOIST MODELS

6.1 General

The response of the composite joist models are compared to the prototype response to evaluate the usefulness of the model. The measured prototype response was obtained from deflection transducers, strain gages, and slip transducers attached to the prototype. The measured responses give an indication of the composite joist behavior and performance. In particular, the composite joist centerline deflection, the top chord and bottom chord centerline strains, and the end slip between the concrete slab and the steel joist are examined.

The applied load vs. centerline deflection plots give an indication of the overall composite joist stiffness and ultimate load capacity. The end slip between the concrete slab and the steel joist top chord gives an indication of the degree of composite action in the system. The bottom chord strain gives an indication of the first yield of the composite joist. Finally, the top chord strain gives an indication of the relative position of the composite joist neutral axis and the point at which composite action is lost.

The applied load vs. centerline deflection plots show the experimental response and the finite element model response. Also shown on the applied load vs. centerline deflection plots are the hand calculations of the yield load and the yield deflection using the method by Chien and Ritchie (1984). The calculations for the yield load and yield deflections for the composite joists

using Chien and Ritchie's method are given in reports by Gibbings, et al. (1991) and Nguyen, et al. (1991). These calculations will be labeled C&R on the plot for brevity and are to be differentiated from the model results.

6.2 Composite Joist Model Results

The results of the seven composite joists modeled are presented in the following sections. Each section will address the load vs. centerline deflection, load vs. end slip, load vs. bottom chord strain, and load vs. top chord strain of the model and the prototype. The results of each model will be discussed and summarized.

6.2.1 Composite Joist CLH-4

The stiffness of model CLH-4 is slightly less than the prototype stiffness as shown in Figure 6.1(a). The model predicts an ultimate load approximately 43% greater than the experimental value.

The model end slip stiffness is less than the actual end slip stiffness. This is shown in Figure 6.1(b). The model and prototype end stud show excessive deflection at approximately the same load level.

The model bottom chord centerline strain is slightly softer than the prototype bottom chord strain. Figure 6.1(c) shows the applied load vs. bottom chord strain plots.

The model centerline top chord strain shown in Figure 6.1(d) indicates that the top chord goes into tension under initial loading and the tension becomes more pronounced near the ultimate load. The prototype shows

little strain until it reaches near the ultimate load where it goes into tension, but to a lesser extent than the model.

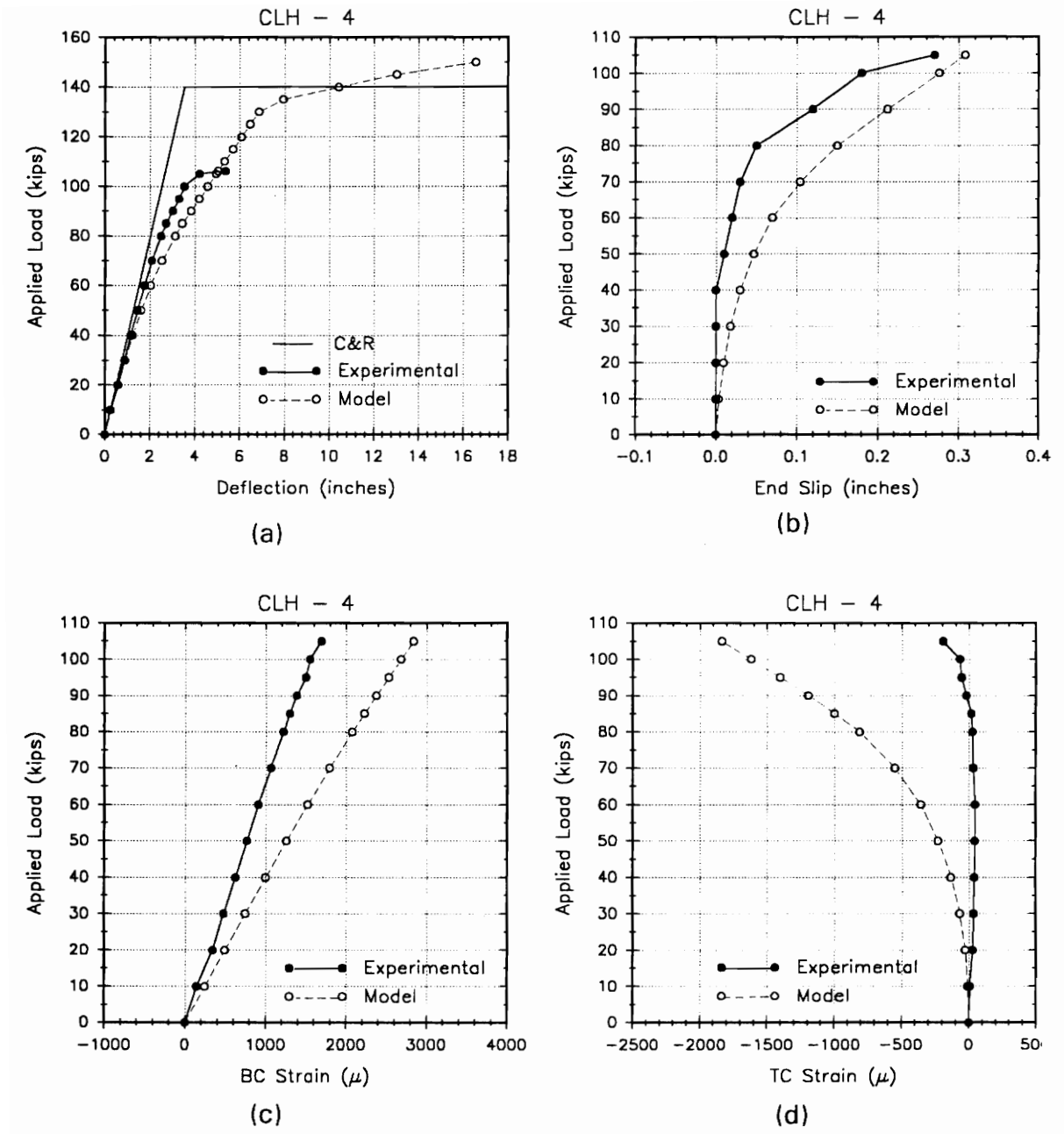

Figure 6.1 Graphs of CLH-4

(a) Load vs. Centerline Deflection, (b) Load vs. End Slip, (c) Load vs. Centerline Bottom Chord Strain, and (d) Load vs. Centerline Top Chord Strain

6.2.2 Composite Joist CLH-5

The model of composite joist CLH-5 is slightly stiffer than the prototype. The model overestimates the ultimate load of the prototype by 12%. Figure 6.2(a) shows the applied load vs. centerline deflection for composite joist CLH-5.

The applied load vs. end slip plot of Figure 6.2(b) shows that the model is stiffer than the prototype. The load at which the model end stud reaches its ultimate capacity would appear to be higher for the model than for the prototype.

Figure 6.2(c) shows the applied load vs. centerline bottom chord strain. The model bottom chord stiffness is less than the prototype bottom chord stiffness. The bottom chord yield strain is shown to be higher for the model than for the prototype.

The applied load vs. top chord strain of Figure 6.2(d) shows very different behavior between the model and the prototype. Under initial loading, both the model and prototype undergo tension. As load increases above 40 kips, the model top chord goes into compression whereas the prototype top chord maintains a fairly constant tension strain. At ultimate load, the behavior of the model and prototype become more pronounced. The model top chord reaches a maximum compressive strain and reverses direction of strain increment under further application of load. The prototype top chord goes further in tension beyond the ultimate load.

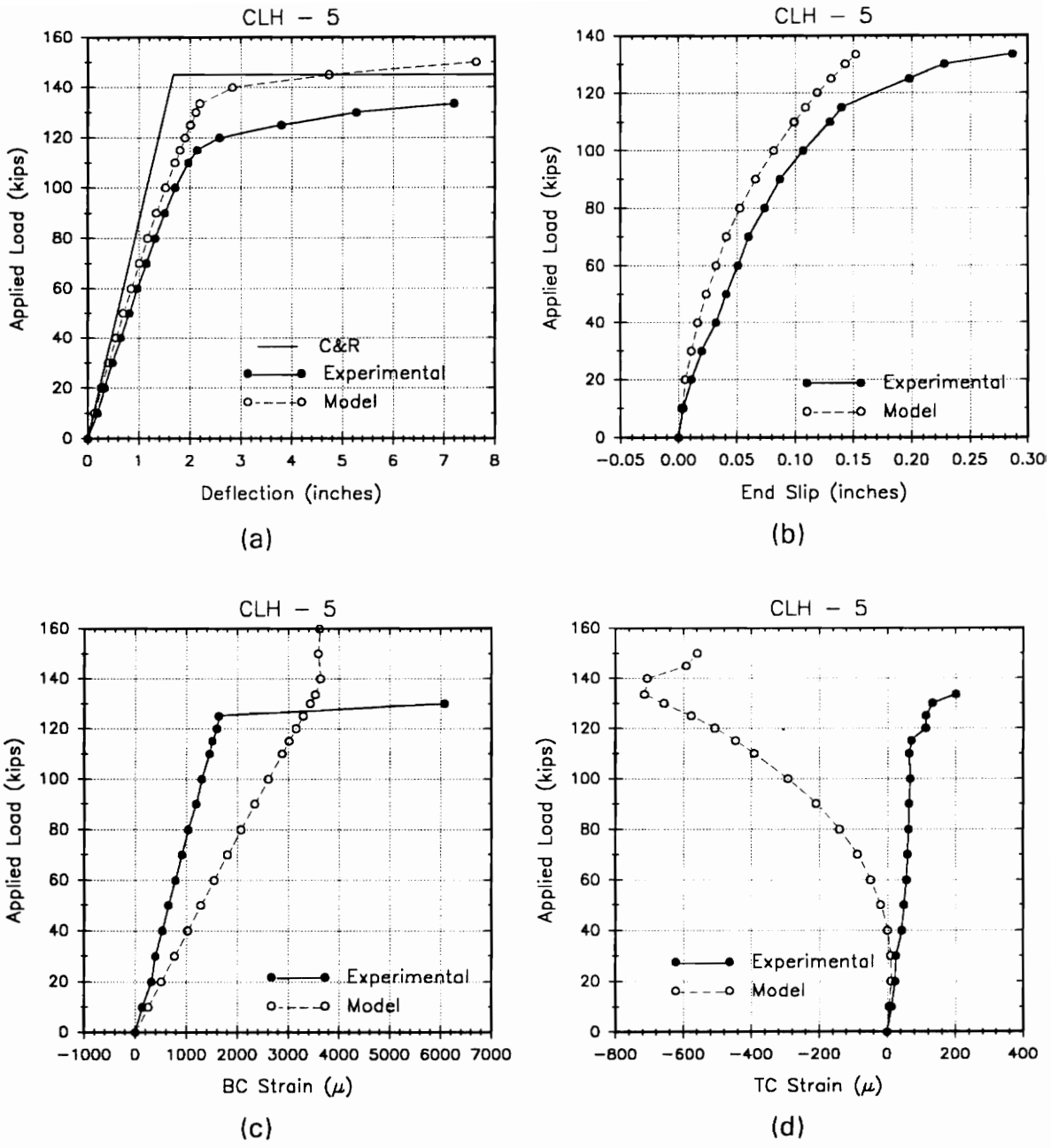

Figure 6.2 Graphs of CLH-5

(a) Load vs. Centerline Deflection, (b) Load vs. End Slip, (c) Load vs. Centerline Bottom Chord Strain, and (d) Load vs. Centerline Top Chord Strain

6.2.3 Composite Joist CLH-6

The model stiffness of composite joist CLH-6 is less than the prototype stiffness as shown in Figure 6.3(a). The model ultimate load, however, agrees well with the prototype ultimate load.

The model end slip stiffness is slightly less than the prototype end slip stiffness. The applied load at which the end stud reaches its ultimate capacity is approximately the same for the model and the prototype. This can be seen in Figure 6.3(b).

The bottom chord strain of the model is greater than the prototype bottom chord strain at any load point. The model bottom chord redistributes load at a higher load level than the prototype. This is illustrated in Figure 6.3(c).

The model top chord strain shows similar behavior to that of the prototype except to a more exaggerated scale. The model top chord goes into tension under load up to a load level of 70 kips and from that point goes into compression up to a load level of 97.5 kips. The prototype top chord goes slightly into tension up to a load level of 50 kips and goes into compression above 50 kips. This is shown in Figure 6.3(d).

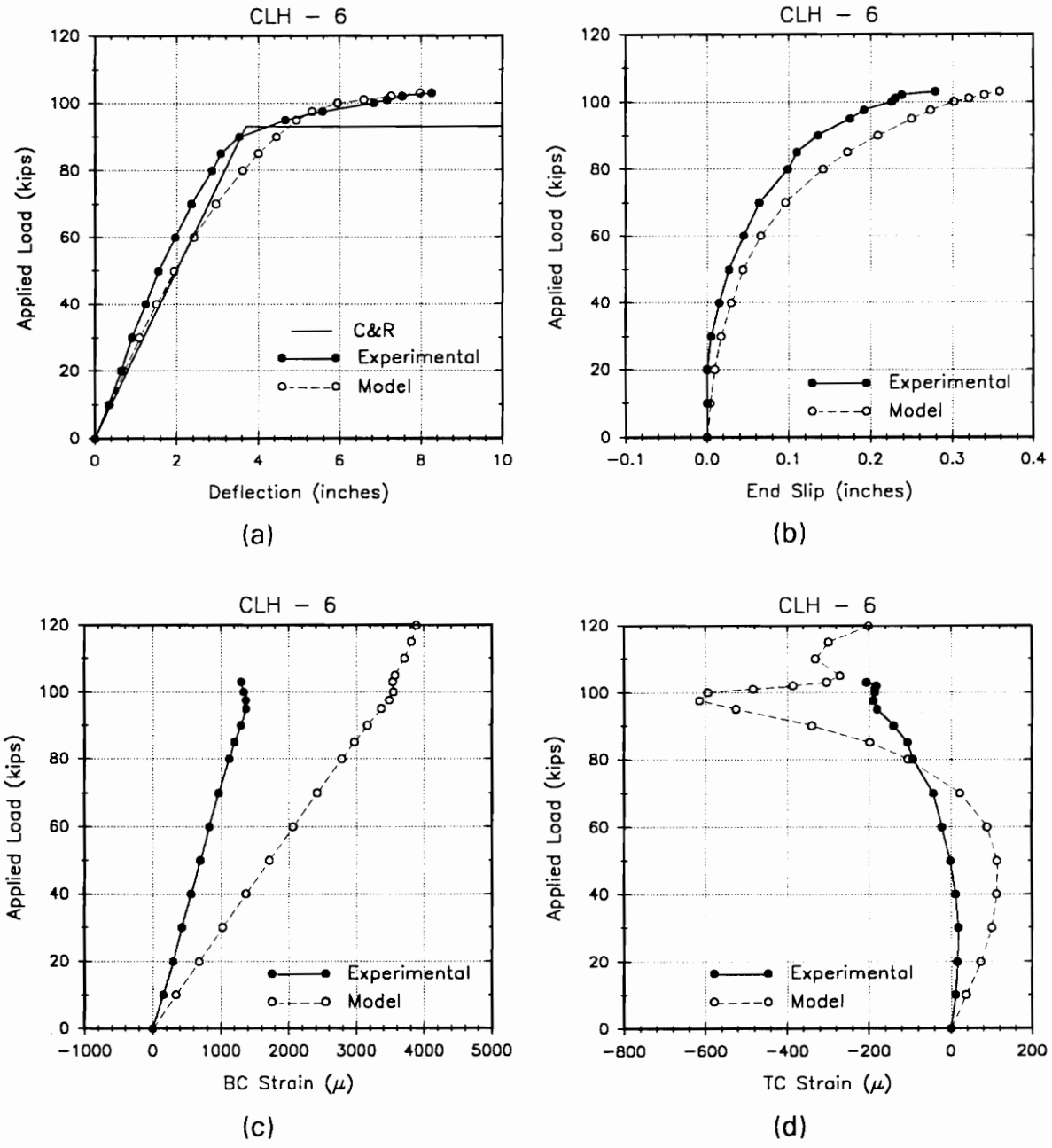

Figure 6.3 Graphs of CLH-6

(a) Load vs. Centerline Deflection, (b) Load vs. End Slip, (c) Load vs. Centerline Bottom Chord Strain, and (d) Load vs. Centerline Top Chord Strain

6.2.4 Composite Joist CLH-7

The load vs. deflection plot of composite joist model CLH-7 agrees well with that of the prototype up to an applied load of 50 kips. This is shown in Figure 6.4(a). Beyond 50 kips, the model stiffness diminishes more rapidly than the prototype stiffness. The ultimate loads of the model and the prototype agree very well.

The model and prototype end slip plots do not agree as well as the centerline deflection plots. From Figure 6.4(b), the model and prototype end slip stiffnesses agree reasonably well up to about 50 kips. Above 50 kips, the prototype stiffness deviates from the model stiffness and actually becomes stiffer from 70 kips to 80 kips. In spite of this, the load where the end stud reaches the ultimate capacity agrees fairly well for the model and the prototype.

The bottom chord stiffness of the model is shown to be less than that of the prototype in Figure 6.4(c). The prototype bottom chord yields at a lower load point than the model bottom chord.

The top chord strains of the model and prototype agree well up to a load point of 40 kips. Beyond 60 kips, the model top chord goes into compression up to 135 kips and reverses in strain increment direction. The prototype top chord maintains a relatively constant strain above 40 kips and goes into further tension at 137 kips. This is illustrated in Figure 6.4(d).

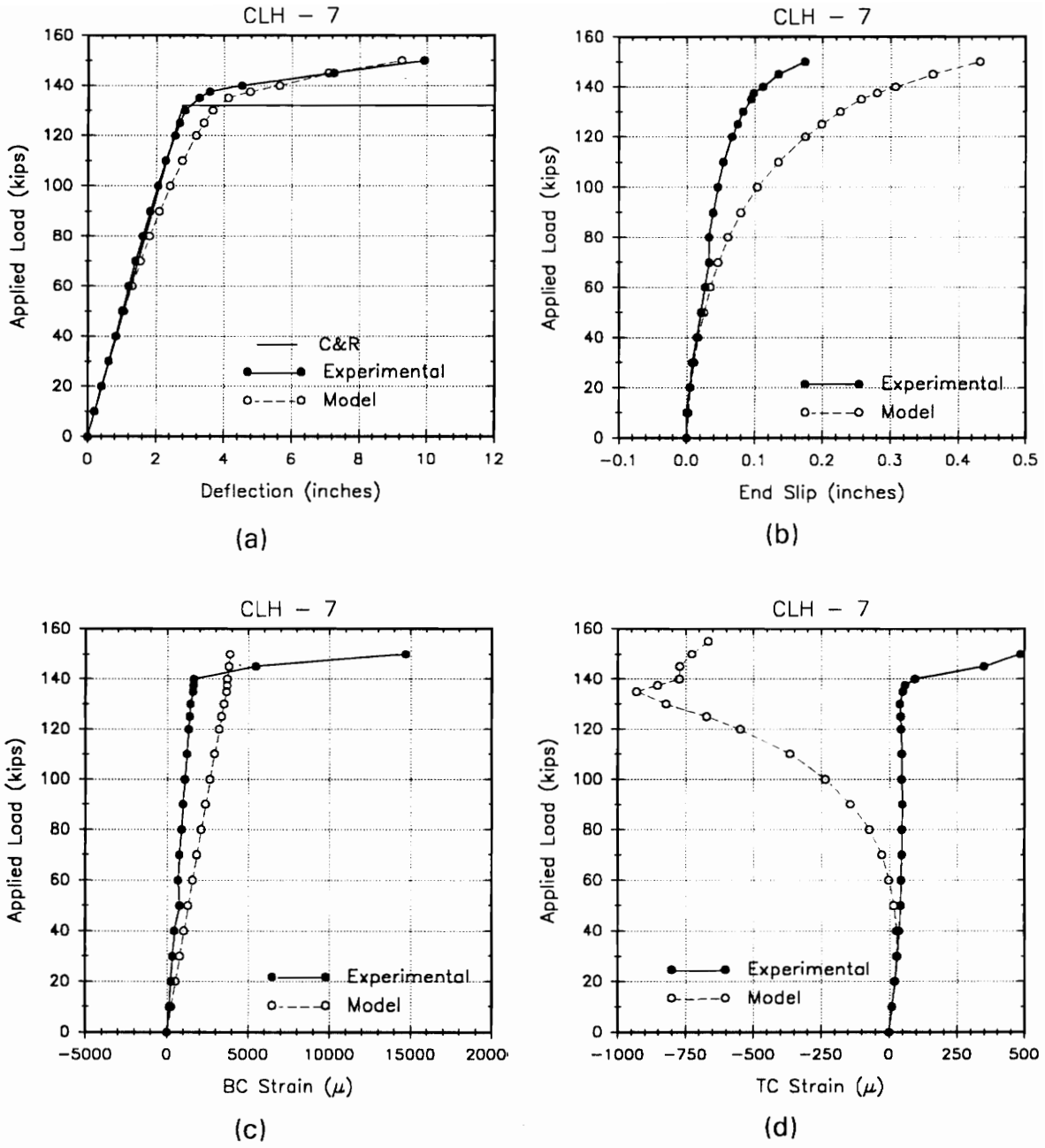

Figure 6.4 Graphs of CLH-7
(a) Load vs. Centerline Deflection, (b) Load vs. End Slip, (c) Load vs. Centerline Bottom Chord Strain, and (d) Load vs. Centerline Top Chord Strain

6.2.5 Composite Joist CLH-8

The model stiffness of composite joist CLH-8 agrees well with the prototype stiffness in the load vs. deflection plot of Figure 6.5(a). The model predicts an ultimate load less than the prototype value. The model ultimate capacity is 145 kips whereas the prototype ultimate capacity is 152 kips.

The model end slip stiffness is less than the prototype as indicated in Figure 6.5(b). The load at which the end stud reaches its ultimate capacity is 3.3% greater for the prototype than for the model.

The model and prototype centerline bottom chord strains agree well for composite joist CLH-8. This is depicted in Figure 6.5(c).

Similarly, Figure 6.5(d) shows reasonably good agreement between the model and prototype centerline top chord strains. For the most part, the model and prototype top chords maintain fairly constant strain near zero up to an applied load of 70 kips. Above 70 kips, the model and prototype top chords go into compression. At an applied load of 130 kips, however, the model top chord strain increment reverses direction and goes into tension above 142 kips.

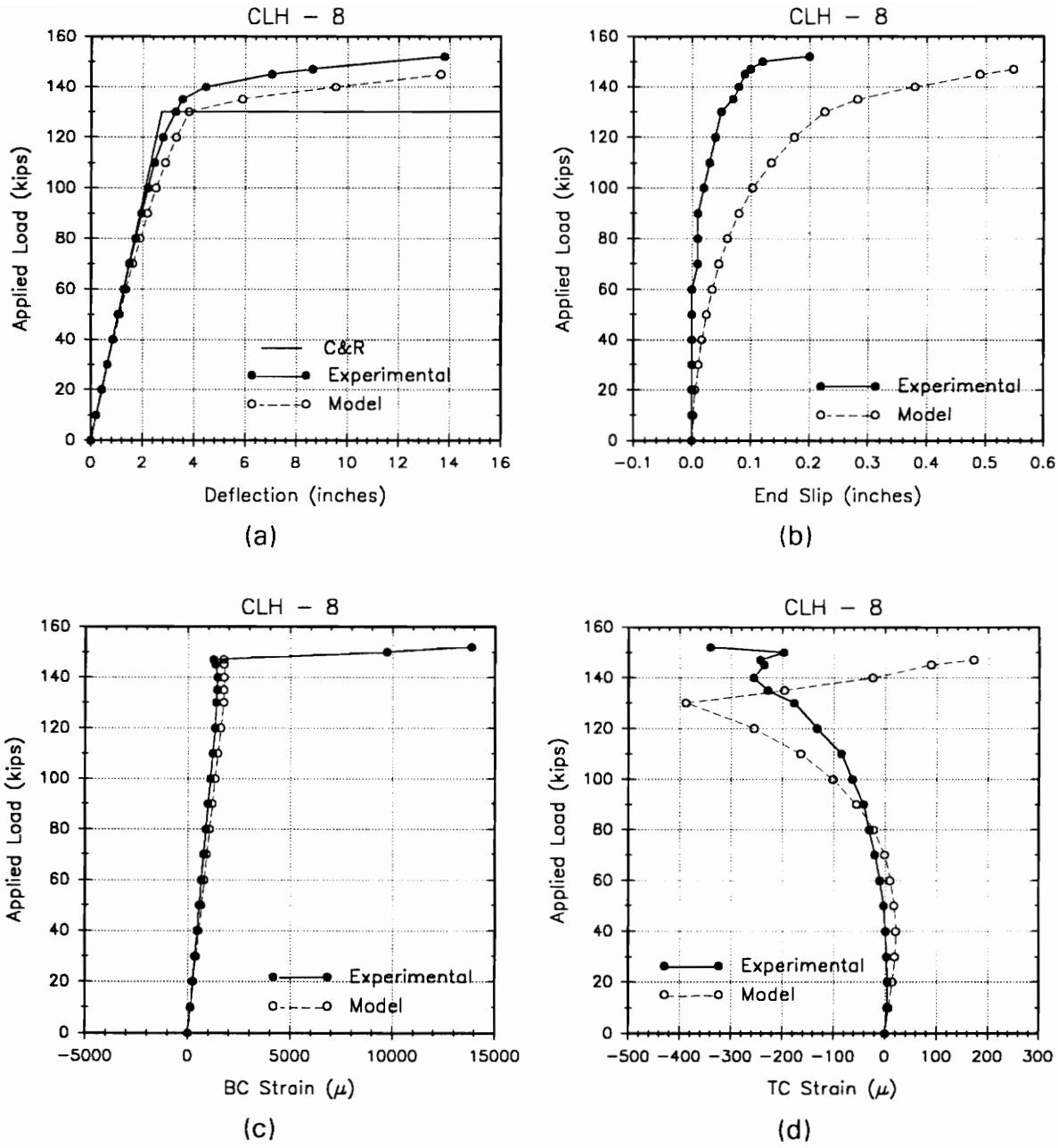

Figure 6.5 Graphs of CLH-8
(a) Load vs. Centerline Deflection, (b) Load vs. End Slip, (c) Load vs. Centerline Bottom Chord Strain, and (d) Load vs. Centerline Top Chord Strain

6.2.6 Composite Joist CLH-9

The load vs. deflection plot of Figure 6.6(a) shows the model to be stiffer than the prototype. The ultimate loads of the model and prototype show reasonably good agreement.

The end slip curves in Figure 6.6(b) show the model to be stiffer than the prototype. The load at which the end stud reaches its ultimate capacity appears to be higher for the model than for the prototype.

The centerline bottom chord stiffness of the model is less than that of the prototype as shown in Figure 6.6(c). The prototype also yields at a lower load than the model.

The centerline top chord stiffness of the model is shown to be less than that of the prototype in Figure 6.6(d). The top chord tensile strain of the model increases at a constant rate until it reaches an applied load of 80 kips, beyond which its rate of increment rises dramatically. The top chord strain of the prototype is fairly constant up to a load of 85 kips. From 85 kips to 95 kips, the prototype chord strain increases in tension. At 95 kips, the prototype top chord strain increment reverses in direction until it reaches a strain of approximately zero.

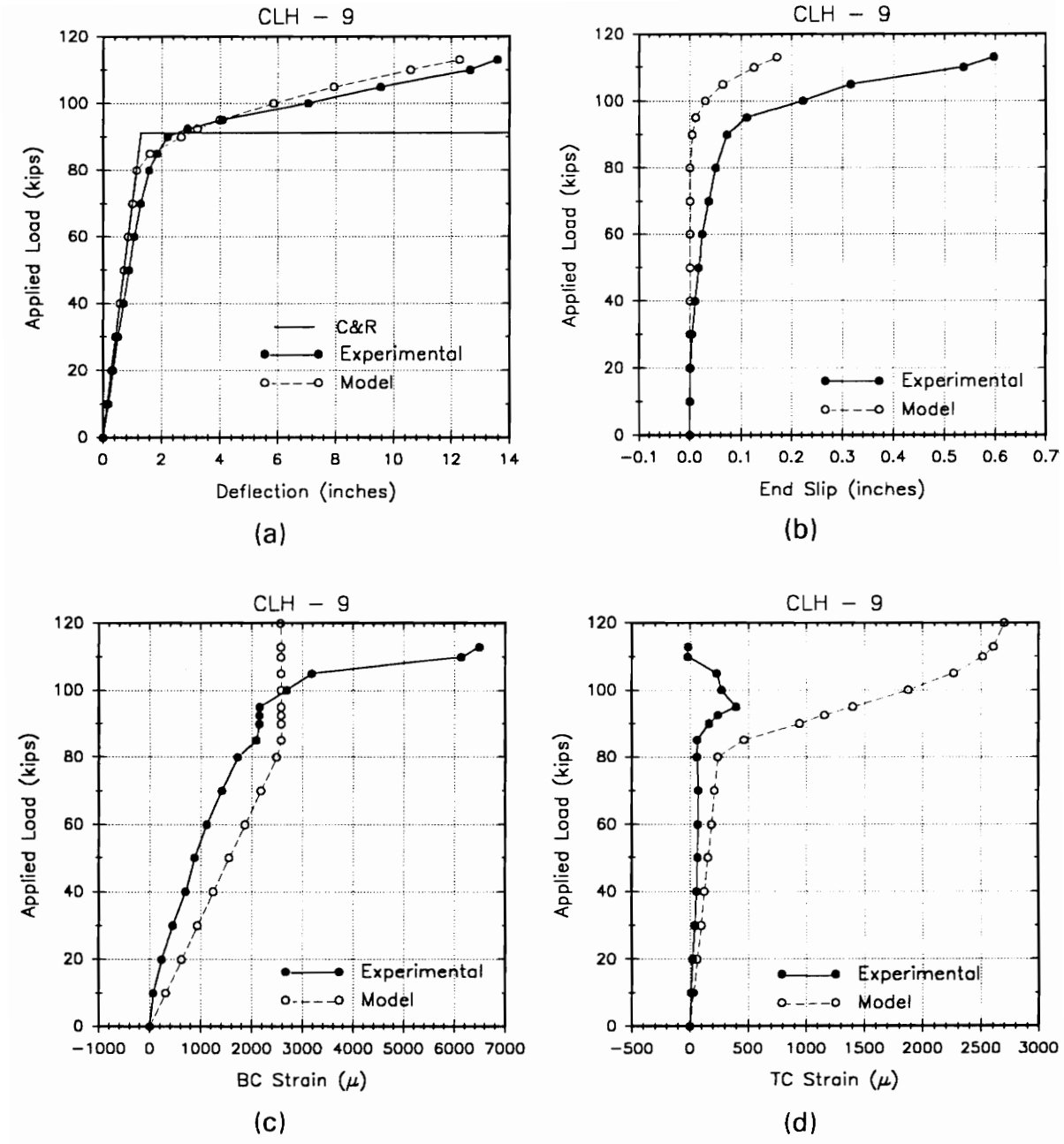

Figure 6.6 Graphs of CLH-9
(a) Load vs. Centerline Deflection, (b) Load vs. End Slip, (c) Load vs. Centerline Bottom Chord Strain, and (d) Load vs. Centerline Top Chord Strain

6.2.7 Composite Joist CLH-11

The model centerline deflection stiffness of composite joist CLH-11 agrees well with the prototype stiffness as indicated in Figure 6.7(a). However, the model overestimates the prototype ultimate capacity by 10%.

The end slip stiffness of the model is less than that of the prototype. The load at which the end stud reaches its ultimate capacity is greater for the model than for the prototype. Figure 6.7(b) shows the applied load vs. end slip curves for the model and the prototype.

The centerline bottom chord stiffness of the model is less than that of the prototype as shown in Figure 6.7(c). Figure 6.7(c) also shows that the prototype bottom chord yields at a lower load than the model bottom chord.

Figure 6.7(d) shows very different behavior between the model and the prototype top chords. The model top chord goes into compression under load and continues in compression up to 92.5 kips of applied load. At 92.5 kips, the model top chord strain increments reverse in direction. The prototype top chord maintains a fairly constant strain near zero up to an applied load of 60 kips. Above 60 kips, the prototype top chord begins to go into compression.

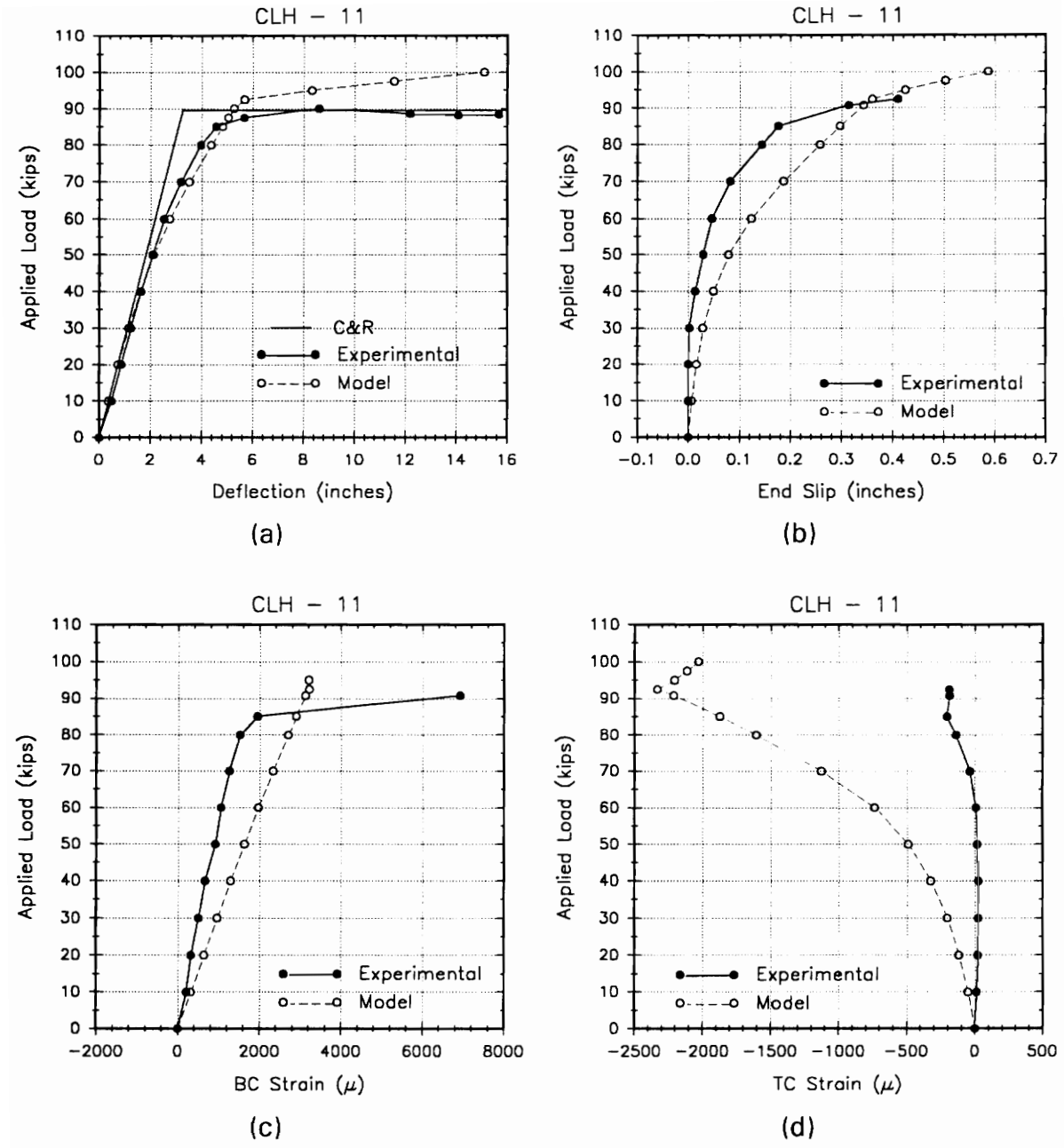

Figure 6.7 Graphs of CLH-11
(a) Load vs. Centerline Deflection, (b) Load vs. End Slip, (c) Load vs. Centerline Bottom Chord Strain, and (d) Load vs. Centerline Top Chord Strain

6.3 Discussion of Model Results

The models proved to be useful in predicting the deflections of the prototypes. In four of the models, CLH-4, CLH-6, CLH-7, and CLH-8, the centerline deflection stiffness of the model was less than that of the prototype. Two of the models, CLH-5 and CLH-9, had a model stiffness that was greater than the prototype stiffness. Composite joist CLH-11 was the only specimen that showed almost exact agreement between the model and prototype stiffness up to the yield load.

The end slip plots of the models gave an indication of the degree of composite action between the concrete slab and the steel joist. The model end slip reflected the behavior of the prototype end slip fairly well. For the most part, the model end slip stiffness was lower than the prototype end slip stiffness. The exceptions were composite joists CLH-5 and CLH-9 where the model end slip stiffness was higher than that of the prototype.

The centerline bottom chord strains of the models were greater than those of the prototypes. The degree of discrepancy between the model and prototype bottom chord strains did not seem to be affected by the amount of slip in the composite joist. One explanation for the discrepancy between the model and prototype bottom chord strains is that the strain gages were not installed at the exact neutral axis of the bottom chord. A more viable explanation is that yielding in the composite joist prototype begins at the panel points in the bottom chord where the webs come together and gradually spreads out to the rest of the member. In other words, the panel points are more highly stressed than the rest of the member since these points are subject to moment, shear and tension. The beam model of the

bottom chord, however, assumes a perfectly straight, prismatic element where the strain is uniform throughout the member, giving the same strain at the panel points and between panel points. This would result in higher strain readings for the model bottom chord.

The same argument for the discrepancy between the model and prototype bottom chord strains can be used for the top chord strains. However, due to the difficulty in determining the exact location of the prototype elastic and plastic neutral axes for nonrigid shear connection, the model top chord strains cannot accurately represent the prototype top chord strains. Consequently, the top chord strains of the model should not be used to predict the prototype top chord strains.

CHAPTER VII

EVALUATION OF RESULTS

7.1 General

The results of the finite element models are evaluated in this section. The evaluation is based on the composite joist applied load vs. centerline deflection response, since this gives a good indication of the overall structural behavior. In particular, the ultimate load capacities of the model and prototype will be compared. The stiffnesses of the model and prototype will also be examined. Finally, the yield load and yield deflection of the models will be evaluated. The theoretical results of previous calculations (Gibbings, et al. 1991; Nguyen, et al. 1991) using Chien and Ritchie's method (1984) will also be compared to the prototype results.

7.2 Composite Joist Ultimate Load Comparison

The ultimate load of the joist is taken as the highest load that the joist can carry without deflecting excessively. A reasonable limit for excessive deflection is L/30, which for a 40 ft. span joist gives a deflection limit of 16 in. Table 7.1 summarizes the ultimate loads of the model and the experimental specimen. All of the models were unconservative in predicting the experimental ultimate load except for model CLH-8. The unconservative models overpredicted the experimental ultimate load from 1% to 43%. For the five of the unconservative models, the overprediction was less than 12%.

Table 7.1 Ultimate Load Capacity Comparisons

TEST	EXPERIMENT ULTIMATE CAPACITY (k)	MODEL ULTIMATE CAPACITY (k)	C&R ULTIMATE CAPACITY (k)	$\frac{P_{Umod}{}^{2}}{P_{Uexp}{}^{1}}$	$\frac{P_{UC\&R}{}^{3}}{P_{Uexp}{}^{1}}$
CLH-4	105	150	140	1.429	1.333
CLH-5	134	150	145	1.119	1.082
CLH-6	103	104	93.1	1.010	0.904
CLH-7	150	152	132	1.013	0.880
CLH-8	152	145	130	0.954	0.855
CLH-9	113	116	91.2	1.027	0.807
CLH-11	91	100	89.5	1.099	0.984

$^{1}P_{Uexp}$ = Experimental ultimate load capacity
$^{2}P_{Umod}$ = Model ultimate load capacity
$^{3}P_{UC\&R}$ = Chien and Ritchie's ultimate load capacity

Model CLH-4, however, overpredicted the experimental ultimate load by 43%. This gross overprediction reveals some limitations of the model. One reason for the overprediction is that the model cannot account for top chord local buckling at the shear stud locations which took place in the experimental specimen. Another reason for the difference between the model and experimental ultimate loads is that the model does not consider shear failure of the studs which were reported in the experimental specimen. The experimental specimen shows failure at a load where shear connector failure occurs leading to subsequent top chord local buckling. The model does not account for the shear connector failure or the top chord

local buckling. Consequently, even though model CLH-4 is less stiff than the experimental specimen, shear connection is maintained in the model with no top chord local buckling. This allows the model bottom chord to be developed in tension up to the ultimate load. Thus, the model yields a higher ultimate load than the experimental specimen.

Not all of the models show the large difference between the model and experimental ultimate loads. In fact, this only shows up in model CLH-4 because the shear connector capacity provided was less than that required to develop the bottom chord in tension (Gibbings, et al. 1991). This caused shear stud failure and subsequent localized stresses in the top chord to develop, resulting in local buckling near the studs. All of the other composite joist tests had sufficient shear connection to develop the bottom chord in tension (Gibbings, et al. 1991; Nguyen, et al. 1991). As a result, the models of the other tests yield more favorable results. Five of the seven models had ultimate loads that differed less than 5% from the prototype ultimate load. Six of the seven models differed less than 12% from the prototype ultimate load.

Chien and Ritchie's ultimate loads for the composite joists previously calculated (Gibbings, et al. 1991; Nguyen, et al. 1991) are also tabulated in Table 7.1. Notice that with the exception of tests CLH-4, CLH-5, and CLH-11, Chien and Ritchie's results are worse than the model results. Chien and Ritchie's ultimate load of CLH-4 overpredicts the prototype ultimate load by 33% as compared to 43% for the model. Chien and Ritchie's method, like the model, assumes that the shear connectors do not fail first. The Canadian code requires that all of the composite joist components be

designed to develop the bottom chord in tension, including the shear connectors. Consequently, the model and Chien and Ritchie's method cannot be used to predict the ultimate load of test CLH-4. Chien and Ritchie's method overpredicts the ultimate load of specimen CLH-5 by 8% as compared to 12% overprediction by the model.

Overall, the models give better predictions of the actual ultimate loads than Chien and Ritchie's method. However, the models tend to be unconservative in predicting the experimental ultimate load whereas Chien and Ritchie's method tends to be conservative. Both methods can give reasonable results, but neither method should be used if the controlling mode of failure is shear connector failure.

7.3 Composite Joist Stiffness Comparison

The model and prototype stiffnesses can be evaluated by comparing the elastic stiffness of their respective load vs. deflection curves. The elastic stiffness of the model and prototype was approximated by fitting a line from the origin to the point at one-half of the ultimate load. Figure 7.1 shows the graphical illustration of the composite joist stiffness. The results of the stiffness calculations are presented in Table 7.2.

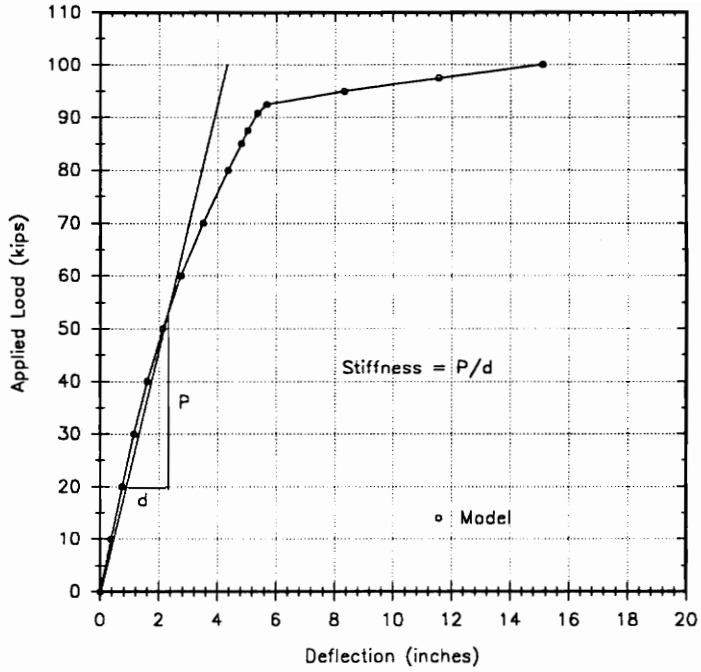

Figure 7.1 Graphical Illustration of Stiffness

Table 7.2 Stiffness Comparisons

TEST	EXPERIMENT STIFFNESS (k/in)	MODEL STIFFNESS (k/in)	C&R STIFFNESS (k/in)	MOD STIF / EXP STIF	C&R STIF / EXP STIF
CLH-4	34.2	31.1	39.7	0.909	1.161
CLH-5	60.9	70.0	87.1	1.149	1.430
CLH-6	32.3	25.8	25.2	0.799	0.780
CLH-7	50.0	44.6	47.4	0.892	0.948
CLH-8	46.3	42.6	47.1	0.920	1.017
CLH-9	56.1	69.6	70.8	1.241	1.262
CLH-11	24.1	24.1	28.7	1.000	1.191

The results of Table 7.2 indicate that the differences between the model stiffness and the experimental stiffness range from 0% to 24%. The cause of the differences between the model stiffness and the experimental stiffness lies in the shear force-deformation modeling of the shear connectors. Referring to the applied load vs. endslip graphs of the composite joists in Chapter VI, the load vs. deflection curve of the model is stiffer than that of the prototype when the shear connector stiffness of the model is greater than that of the prototype. The model stiffness inaccuracies lie not with the model components, but rather with the inaccuracies of the shear force-slip equation of Ollgaard, et al. (1971) used in the model. Despite the inaccuracies of the Ollgaard, et al. shear force-slip equation, it is the best representation for the shear stud stiffness presently available.

Another point to reinforce the fact that the errors in the model stiffness are due to the shear force-slip equation is that the discrepancy between the model and prototype stiffnesses was not affected by the position of the shear connectors. This is illustrated by composite joists CLH-5, CLH-6, and CLH-9. Composite joist CLH-5 had shear studs installed only in the strong position and a ratio of the total shear stud capacity to the bottom chord tensile capacity of 1.27 (Gibbings, et al. 1991). The model had a stiffer load vs. slip curve than the prototype. Composite joist CLH-6 also had shear studs installed only in the strong position and its ratio of the total shear stud capacity to the bottom chord tensile capacity was 1.39 (Gibbings, et al. 1991) which is greater than that of CLH-5. Yet, the load vs. endslip curve of the model is less stiff than that of the prototype. On

the other side of this, composite joist CLH-9 had shear studs installed in alternating strong and weak positions and the ratio of the total shear stud capacity to the bottom chord tensile capacity was 1.37 (Nguyen, et al. 1991). Yet, the load vs. slip curve of the model is stiffer than that of the prototype. From this illustration, it can be concluded that neither the position of the shear connectors nor the amount of shear connection above that required to develop the bottom chord tensile capacity will determine whether the model centerline deflection is stiffer or softer than the prototype. Rather, it will be controlled by the accuracy of the Ollgaard shear force-slip equation.

Despite the differences between the model and the prototype centerline deflection stiffnesses, a comparison with Chien and Ritchie's calculated stiffness values should give a better idea of how well the models performed. Chien and Ritchie's stiffness values can be found in reports by Gibbings, et al. (1991) and Nguyen, et al. (1991). Table 7.2 shows Chien and Ritchie's stiffness values and their ratios with respect to the experimental stiffness values. Chien and Ritchie's values compare less favorably with the experimental stiffness values than the models, with the exception of CLH-7 and CLH-8. Model CLH-7 underpredicts the experimental stiffness by 11% whereas Chien and Ritchie's method underpredicts it by 5%. On the other hand, model CLH-8 underpredicts the experimental stiffness by 8%, but Chien and Ritchie's method overpredicts the actual stiffness by 2%.

Overall, the model gives closer values to the experimental stiffness than Chien and Ritchie's method. In addition, the stiffness values of the

model tend to be lower than the experimental values whereas Chien and Ritchie's stiffness values tend to be higher than the experimental values. The model, therefore, should be used when accuracy for stiffness is required.

7.4 Composite Joist Yield Load and Deflection Comparison

The yield load and yield deflection represent the transition point of the structure loading from elastic behavior to plastic behavior. The yield load and yield deflection is obtained by fitting a line through the elastic portion of the graph and a line through the plastic portion. The intersection of these two lines gives the yield load and yield deflection. The graphical determination of the yield load and yield deflection of a composite joist is shown in Figure 7.2.

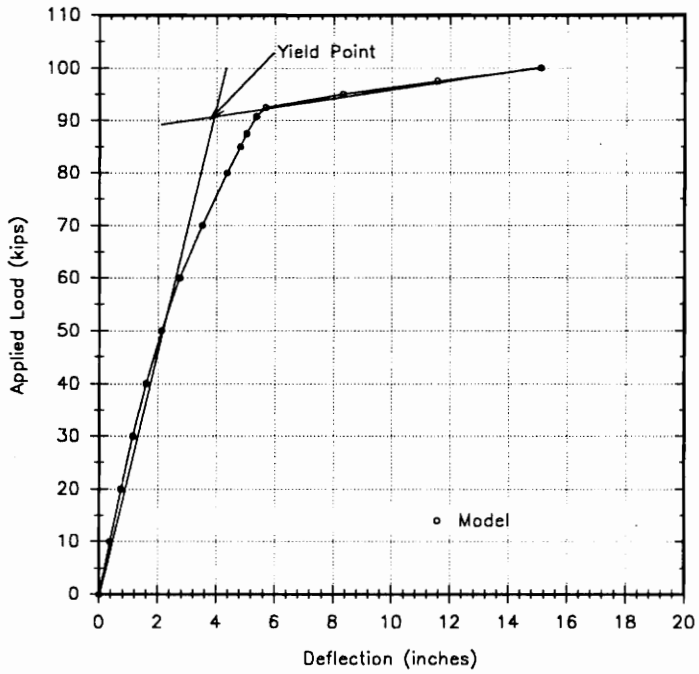

Figure 7.2 Graphical Determination of Yield Point

Table 7.3 shows the yield loads of the prototype, the model, and Chien and Ritchie's method. The model yield loads are in good agreement with the experimental yield loads with the exception of CLH-4 and CLH-5. Chien and Ritchie's method gives values similar to the model yield loads.

Table 7.3 Yield Load Comparisons

TEST	EXPERIMENT YIELD LOAD (k)	MODEL YIELD LOAD (k)	C&R YIELD LOAD (k)	$\frac{P_{Ymod}{}^{2}}{P_{Yexp}{}^{1}}$	$\frac{P_{YC\&R}{}^{3}}{P_{Yexp}{}^{1}}$
CLH-4	104	128	140	1.231	1.346
CLH-5	122	138	145	1.131	1.189
CLH-6	90.5	96.5	93.1	1.066	1.029
CLH-7	136	133	132	0.978	0.971
CLH-8	140	132	130	0.943	0.929
CLH-9	90.5	92	91.2	1.017	1.008
CLH-11	88	92	89.5	1.045	1.017

$^{1}P_{Yexp}$ = Experimental yield load
$^{2}P_{Ymod}$ = Model yield load
$^{3}P_{YC\&R}$ = Chien and Ritchie's yield load

Table 7.4 shows the yield deflections for the prototype, the model, and Chien and Ritchie's method. The model yield deflections agree reasonably well with the experimental yield deflections with the exception of CLH-4, CLH-6, and CLH-9. Chien and Ritchie's calculations do not compare quite as well with the experimental yield deflections.

Table 7.4 Yield Deflection Comparisons

TEST	EXPERIMENT YIELD DEFL. (in)	MODEL YIELD DEFL. (in)	C&R YIELD DEFL. (in)	$\frac{D_{Ymod}}{D_{Yexp}}$[2][1]	$\frac{D_{YC\&R}}{D_{Yexp}}$[3][1]
CLH-4	3.05	4.20	3.53	1.377	1.157
CLH-5	2.00	1.90	1.67	0.950	0.835
CLH-6	2.80	3.60	3.69	1.286	1.318
CLH-7	2.70	2.90	2.78	1.074	1.030
CLH-8	3.00	3.10	2.75	1.033	0.917
CLH-9	1.60	1.30	1.29	0.813	0.806
CLH-11	3.60	3.70	3.26	1.028	0.906

[1] D_{Yexp} = Experimental yield deflection
[2] D_{Ymod} = Model yield deflection
[3] $D_{YC\&R}$ = Chien and Ritchie's yield deflection

CHAPTER VIII

SUMMARY, CONCLUSIONS, AND RECOMMENDATIONS

8.1 Summary

Seven composite joist tests were modeled using a general purpose finite element program, ANSYS. The models were limited to those tests where the shear stud position in the steel deck were known, since this proved to be an important modeling consideration. The models accounted for incomplete interaction between the concrete slab and the steel joist. This was achieved by using an infinitely stiff stud element with a spring element at its base allowing translation only in the horizontal direction. The Ollgaard, et al. (1971) shear force-deformation equation was used to model the spring stiffness. Figure 4.1 shows the typical finite element model.

The elastic and plastic behavior of the composite joist was modeled by using elastic-plastic beam elements for the top and bottom chords of the steel joist. The web members of the steel joist only needed to be modeled as elastic elements because they were overdesigned to develop the bottom chord tensile capacity. Overall, the model behavior compared reasonably well with the prototype behavior. The finite element model is relatively easy to generate and can be used to predict the deflections and ultimate load capacity of a composite joist, though it tends to give unconservative values for the ultimate load capacity.

8.2 Conclusions

From the seven composite joist tests modeled in this report, the following conclusions are made:

1. The Ollgaard, et al. (1971) shear force-deformation equation gives a reasonable representation of the actual shear stud force-slip behavior. The use of the Ollgaard, et al. equation required that the AISC ultimate shear capacity for studs be factored by 0.65 for studs in the strong position and 0.50 for studs in the weak position. The use of these factors were determined from push off tests and point to the need of push-off tests to verify the shear stud force-deformation equation used for modeling.

2. The model gives a reasonable prediction, i.e. less than 12 % difference, of the ultimate load capacity of the composite joist though it tends to be unconservative.

3. The model centerline deflection compares well with the actual deflection. Moreover, the model generally gives more accurate deflection values than Chien and Ritchie's method. The model tends give higher centerline deflection values than the experimental results, whereas Chien and Ritchie's method tends to give lower deflection values than the experimental results.

4. The model gives good prediction values of the yield load and yield deflection of the composite joist when shear connector failure or top chord local buckling did not occur.

5. The model and Chien and Ritchie's method give similar results for the yield load of the composite joist.

6. The model and Chien and Ritchie's method give poor prediction values for the ultimate load capacity and the yield load of the composite joist when the controlling mode of failure was failure of the shear studs and top chord local buckling. This was the case for composite joist CLH-4.

7. The model tends to give higher strain values for the bottom chord than the actual structure.

8. The model is not accurate in predicting the top chord strains of the steel joist.

8.3 Recommendations

The following recommendations are made based on the finite element analyses of this study:

1. Models of long span composite joists should include the slip that occurs between the concrete slab and steel joist due to the shear connector flexibility. The Ollgaard, et al. (1971) shear force-deformation equation is suitable for modeling the slip of headed shear studs.

2. The AISC ultimate shear capacity for studs should be factored by 0.65 for studs in the strong position and 0.50 for studs in the weak position before being applied to the Ollgaard, et al. shear force-deformation equation based on push-off test by Sublett (1991).

3. Both the top and bottom chords should be modeled as elastic-plastic elements since these members are subject to yielding. The web members, however, need not be modeled as plastic elements since these are designed to develop the bottom chord up to its yield capacity.

4. The finite element model presented in this study should not be used to predict the ultimate load capacity of the composite joist if the controlling mode of failure is shear stud failure.

5. Though the model gives more accurate values for ultimate load capacity than Chien and Ritchie's method, Chien and Ritchie's method may be better suited for design since it tends to be conservative whereas the model ultimate load capacity tends to be unconservative.

6. The model stiffness values are more accurate than Chien and Ritchie's method and, therefore, should be used for stiffness predictions of the composite joist.

7. The model should not be used to predict the top chord strain values of the steel joist. However, the model may be used to predict the bottom chord strain values since the model tends to be conservative in this respect.

8.4 Future Studies

Areas of possible improvements in future finite element studies of composite joists include:

1. For composite joists where top chord local buckling occurs at an early stage of the structure loading, refining the top chord elements may give better ultimate load capacity values.

2. Though the webs are overdesigned in the composite joist, the web members may buckle above the yield load. Web lateral buckling may be modeled by introducing and eccentricity in the web member and refining the

web element mesh. This would give better ultimate load capacity values where lateral web buckling controls in the plastic loading.

3. A method should be incorporated into the finite element program to model shear stud failure by using a contact element. If the ultimate strain is exceeded, the contact element would separate.

4. The eccentricities of the welded joints in the steel joist may be accounted for by adding more elements at these joints. This would be important in modeling the buckling load of the web members.

5. Though concrete cracking and crushing are not controlling modes of failure in the composite joist tests in this study, these properties may need to be incorporated in studies where they do control.

REFERENCES

American Concrete Institute. (1989). *Building Code Requirements for Reinforced Concrete (ACI 318-89) and Commentary (ACI 318R-89).* Detroit, Michigan.

American Institute of Steel Construction. (1989). *Manual of Steel Construction: Allowable Stress Design*. 9th Ed. Chicago, Illinois.

American Institute of Steel Construction. (1986). *Manual of Steel Construction: Load and Resistance Factor Design*. 1st Ed. Chicago, Illinois, Specification I5.3.

Argyris, J. H. and Kelsey, S. (1960). *Energy Theorems and Structural Analysis.* Butterworths, London.

Arizumi, Y. and Hamada, S. (1981). "Elastic-Plastic Analysis of Composite Beams with Incomplete Interaction by Finite Element Method." *Computers and Structures 14*, 453-462.

Azmi, M. H. (1972). *Composite Open-Web Trusses with Metal Cellular Floor*. M.E. Thesis, McMaster University, Hamilton, Ontario, Canada.

Canadian Institute of Steel Construction. (1984). *Handbook of Steel Construction*. 4th Ed., Toronto, Ontario.

Chien, E. Y. L. and Ritchie, K. L. (1984). *Design and Construction of Composite Floor Systems*. Canadian Institute of Steel Construction.

Cook, R. D., Malkus, D. S., and Plesha, M. E. (1989). *Concepts and Applications of Finite Element Analysis*. 3rd Ed. John Wiley and Sons, New York.

Courant, R. (1943). "Variational Methods for the Solution of Problems in Equilibrium and Vibrations." Bulletin of the American Mathematical Society 49, 1-23.

Curry, J. H. (1988). *Full Scale Tests on Two Long-Span Composite Open-Web Steel Joists*. M.S. Thesis, University of Minnesota, Minnesota, U.S.A.

Gibbings, D. R., Easterling, W. S., and Murray, T. M. (1991). *Evaluation of Long Span Composite Joists*. Research Report, Report No. CE/VPI-ST91/02, Virginia Tech, Blacksburg, VA.

Hamada, S. and Arizumi, Y. (1977). "Finite Element Analysis of Continuous Composite Beams with Incomplete Interaction." *Transactions of JSCE 9*, 64-67.

Hirst, M. J. S. and Yeo, M. F. (1980). "The Analysis of Composite Beams Using Standard Finite Element Programs." *Computers and Structures 11*, 233-237.

Johnson, R. P. and Buckby, R. J. (1986). *Composite Structures in Steel and Concrete*. 2nd Ed., Vol. 2, Collins, London, 78-101.

Kitoh, H. and Sonoda, K. (1991). "Forces on the Studs in a Steel Plate and Concrete Slab." IABSE Report Vol. 60, Zurich, Switzerland,185-190.

McCarthy, W.C. and Melhem, A. Q. (1988). "Elasto-Plastic Analysis of Composite Steel-Concrete Superstructures." *Computers and Structures 29*, 601-610.

Newmark, N. M., Seiss, C. P., and Viest, I. M. (1951). "Test and Analysis of Composite Beams with Incomplete Interaction." Proceedings of the Society of Experimental Stress Analysis, Vol. 9, No. 1, 75-92.

Nguyen, S. T., Easterling, W. S., and Murray, T. M. (1991). *Further Studies on Composite Long Span Open-Web Steel Joists*. Research Report, Report No. CE/VPI-ST91/12, Virginia Tech, Blacksburg, VA.

Ollgaard, J. G., Slutter, R. G., and Fisher, J. W. (1971). "Shear Strength of Stud Connectors on Light-weight Concrete and Normal Weight Concrete." *Engineering Journal of AISC 5*, 55-64.

Razaqur, A. G. and Nofal, M. (1989). "A Finite Element for Modeling the Nonlinear Behavior of Shear Connectors in Composite Structures." *Computers and Structures 32*, 169-174.

Razaqur, G. A. and Nofal, M. (1990). "Analytical Modeling of Nonlinear Behavior of Composite Bridges." *Journal of Structural Engineering 116*, 1715-1733.

Salmon, C. G. and Johnson, J. E. (1990). *Steel Structures: Design and Behavior Emphasizing Load and Resistance Factor Design*. 3rd Ed. Harper and Row. New York.

Sublett, C. N. (1991). *Strength of Welded Headed Studs in Ribbed Metal Deck on Composite Joists*. M.S. Thesis, Virginia Tech, Blacksburg, VA.

Swanson Analysis Systems, Inc. (1989). SASI Revision 4.4, User's Manual Vol. I and Vol. II.

Swanson Analysis Systems, Inc. (1989a). SASI Revision 4.4, Theoretical Manual.

Turner, M. J., Clough, R. W., Martin, H. C., and Topp, L. J. (1956). "Stiffness and Deflection Analysis of Complex Structures." *Journal of Aerospace Science 23*, 805-823.

Wegmuller, A. W. and Amer, H. N. (1977). "Nonlinear Response of Composite Steel-Concrete Bridges." *Computers and Structures 7*, 161-169.

Wegmuller, A. W. (1977). "Overload Behavior of Composite Steel-Concrete Bridges." *Proceedings of ASCE 103*, 1799-1819.

Yam, L. C. P. and Chapman, J. C. (1972). "The Inelastic Behavior of Continuous Composite Beams of Steel and Concrete." *Proceedings of the Institute of Civil Engineers Part 2*, London, England, 487-501.

VITA

Son T. Nguyen was born in Danang, Vietnam on the 8th of April in the year of 1968. He graduated from Cheyenne Central High School in Wyoming on June of 1986. He received his Bachelor of Science degree in Civil Engineering from the University of Wyoming in May of 1990. He went on to pursue a Master of Science degree in Civil Engineering at Virginia Polytechnic Institute and State University in Blacksburg, Virginia in the fall of 1990.